DISCLAIMER

This document was prepared as an account of work sponsored by the United States Government. While this document is believed to contain correct information, neither the United States Government nor any agency thereof, nor the Regents of the University of California, nor any of their employees, makes any warranty, express or implied, or assumes any legal responsibility for the accuracy, completeness, or usefulness of any information, apparatus, product, or process disclosed, or represents that its use would not infringe privately owned rights. Reference herein to any specific commercial product, process, or service by its trade name, trademark, manufacturer, or otherwise, does not necessarily constitute or imply its endorsement, recommendation, or favoring by the United States Government or any agency thereof, or the Regents of the University of California. The views and opinions of authors expressed herein do not necessarily state or reflect those of the United States Government or any agency thereof or the Regents of the University of California.

Redox Flow Batteries, a Review

Adam Z. Weber*[,1], Matthew M. Mench[2], Jeremy P. Meyers[3], Philip N. Ross[1], Jeffrey T. Gostick[4], Qinghua Liu[2]

[1]Environmental Energy Technologies Division, Lawrence Berkeley National Laboratory, Berkeley, CA 94720

[2]Department of Mechanical, Aerospace and Biomedical Engineering, University of Tennessee, Knoxville, Tennessee

[3]Department of Mechanical Engineering, The University of Texas, Austin, Texas

[4]Department of Chemical Engineering, McGill University, Montreal, Quebec

Redox flow batteries are enjoying a renaissance due to their ability to store large amounts of electrical energy relatively cheaply and efficiently. In this review, we examine the components of redox flow batteries with a focus on understanding the underlying physical processes. The various transport and kinetic phenomena are discussed along with the most common redox couples.

Keywords: flow battery, redox, regenerative fuel cell, flow cell, vanadium

*Corresponding author: azweber@lbl.gov; phone: 510-486-6308; fax: 510-486-4773

1. Introduction

Renewable-energy sources, such as solar and wind, are being deployed in larger numbers than ever before, but these sources are intermittent and often unpredictable. These characteristics limit the degree to which utilities can rely upon them, and, as such, renewables currently comprise a small percentage of the primary power sources on the US electrical grid. Analysis suggests that an electric grid could become destabilized if non-dispatchable renewable energy exceeds 20 percent of the energy-generation capacity without energy storage [1]. However, many utilities are mandating renewable portfolios approaching this level of deployment, thus there is a pressing need for storage technologies to complement and enable renewable standards. Other than capacitors, however, there is no way to store electrical energy as such. Instead, if electricity is to be stored, it must first be converted to some other form of energy. There are some technologies that enable practical storage of energy at their current levels of deployment, but only a very small fraction of North American power plants employ such technology [2]. To ensure that renewable energy succeeds in delivering reliable power to US consumers, the nation needs cost effective and reliable storage at the grid scale.

Conventional rechargeable batteries offer a simple and efficient way to store electricity, but development to date has largely focused on transportation systems and smaller systems for portable power or intermittent backup power; metrics relating to size and volume are far less critical for grid storage than in portable or transportation applications. It therefore stands to reason that optimizing battery performance over a different set of variables might result in an implementation that delivers superior performance for reduced cost. Batteries for large-scale grid storage require durability for large numbers of charge/discharge cycles as well as calendar life, high round-trip efficiency, an ability to respond rapidly to changes in load or input, and

reasonable capital costs [3]. Redox flow batteries (RFBs) or redox flow cells (RFCs), shown schematically in Figure 1, promise to meet many of these requirements [4].

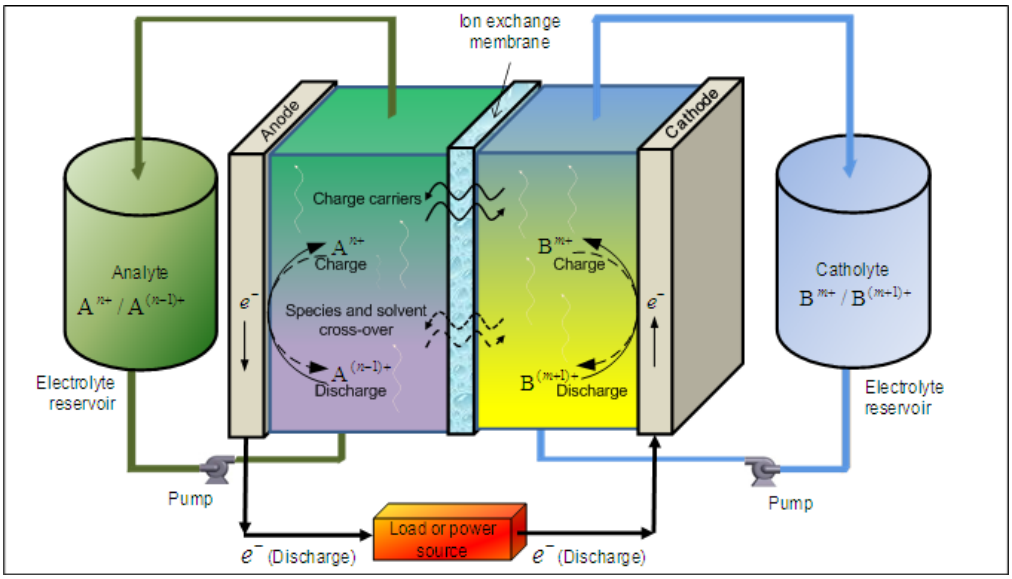

Fig. 1. A schematic diagram of a redox flow battery with electron transport in the circuit, ion transport in the electrolyte and across the membrane, active species crossover, and mass transport in the electrolyte.

As shown in Figure 1, a key component of RFBs is the ability to separate power and energy. The power is controlled by the stack while the energy is stored within the separated reactants. Thus, one can optimize over a greater range of variables and storage can be increased with relatively ease and minimal cost compared to the stack, which is typically the most expensive system component. To examine the technologies that are under development to meet the cost requirements of the marketplace and enable wide-scale storage, we consider the existing portfolio of RFB storage technologies and the possibilities of each. To that end, we introduce the various technologies and discuss in more depth the general attributes and concerns facing RFBs. The overall purpose of this review is to examine systemic issues for the field of RFBs, and not just examine a specific chemistry or the various proposed RFBs. Excellent reviews of these

latter issues and energy storage for the grid in general can be found in the literature [5-8]. The structure of this paper is as follows. After an introduction and short overview of the various major RFBs, the kinetic and transport issues are examined in turn. Next, some overall electrode/cell modeling and designs are reviewed. Finally, some comments about future research needs are made. It should be noted that this review is focused on cell-level issues and RFB chemistries, therefore issues of system integration and components are not examined in depth, although they can be critically important for system commercialization. Before discussing the various RFB chemistries, it is worthwhile to examine their current major applications

1.1 Grid-Storage Needs

The present electric grid constitutes an enormous physical infrastructure, with a near-instantaneous transmission of value from primary power sources and generation assets to end users and almost no storage capability. Because of this dearth of storage, the existing grid must conform to fluctuations in customer demand, resulting in the construction of power plants that may only operate for 100 hours a year or less and can account for up to 30 MWh in capacity [9]. These generators are dispatched to respond to small oscillations in demand over very short time scales of less than 1 hour. They are also turned on and sped up to meet increasing load during the peak time of the day, and, at the other extreme of wastefulness, brought on by the lack of storage. For example, wind energy is wasted because of the inability to dispatch wind power at night when wind generation is at a maximum but customer demand is at a minimum; thus, there is a significant value added by the incorporation of storage [10]. Similarly, photovoltaics and solar-energy implementation will also require arbitrage since although the solar radiation received terrestrially in about one hour is sufficient to meet worldwide energy requirements for a year, the sun does set daily. Storage is a vital tool that would uncouple customer demand from the

generation side of the grid, thereby allowing vital flexibility in control and maintenance of the electric grid. To date, however, energy storage comprises only about 2% of the installed generation capacity in the U.S. Because of differences in government policy and more favorable economics, storage plays a larger role in Europe and Japan, at 10% and 15%, respectively [11].

The current worldwide electric generation capacity was estimated to be about 20 trillion kilowatt-hours in 2007 [12]. More than two-thirds of the current mix is from some form of fossil fuel, with most of the balance coming from nuclear and hydroelectric power generation; at present, only about 3% comes from renewable-energy technologies. Furthermore, developing economies and electrification of the transportation sector both point to strong year-over-year growth in terms of electrical demand. While coal is already the primary source of power in the US electricity sector, there are concerns that it will become a larger portion of electricity production as increased global demand competes for cleaner resources like natural gas. Coal is, of course, the most carbon-intensive resource used in this sector; however, while debate continues about how to address anthropogenic global warming gas emissions from a policy standpoint, coal plants are less capable of handling transient loads than the "peaker" plants that largely sit idle and which are deployed only to handle the peak loads. Growing demand implies not only an increase in the base load, which might be handled by coal if government and the energy sector choose not to prioritize carbon-emissions reductions, but also to larger peak loads, which will either require more intermittent generation assets or storage.

In addition to improvements in resiliency that can enable increased renewable-energy generation, integration of storage into the smart grid also promises to enable greater system efficiency, even with existing generation assets. The Electric Power Research Institute has completed a study that suggests that the widespread adoption of smart grid technologies could

yield a 4% reduction in energy use by 2030 [13], roughly equivalent to eliminating the emissions of 50 million cars. Beyond the emissions impact, that savings translates to more than $20 billion annually for utility customers nationwide. With a more robust and efficient system, and more data about demand patterns, it will be easier for utilities to manage the integration of intermittent renewable-energy sources. Energy storage can also support requirements for reserve generation in place of fossil-fuel-based facilities, yielding zero emissions and lowered operating costs.

It seems apparent that being able to harvest energy from more diverse sources, and being able to deploy this energy to the end user when it is demanded, should lower operating costs and promote the robustness and quality of power on the grid. Why then, is the penetration of storage onto the grid so small? The answer is primarily cost. There are multiple costs associated with the installation and operation of a RFB system: one must consider the operation and maintenance costs, as well as up-front capital costs and life-cycle costs. Because of the decoupling of energy and power in RFB configurations, we can consider both cost per unit of power generation/storage capability ($/kW) and the cost per unit of energy-storage capacity ($/kWh). We note that the cost per unit energy storage is not the incremental cost of producing or storing that energy as would be expected in a utility bill, but the cost per unit of energy-storage capacity. In addition to costs, robust system lifetimes of ~10 years, high efficiency, and cyclic durability are necessary for grid-level storage.

Different applications have different acceptable costs, and the total power and total duration of storage provided will differ from application to application. As such, it is difficult to target a single metric that can concisely address the ultimate cost target for grid-based storage. The table below, from a report prepared by the Nexight Group based upon a workshop convened by Sandia, PNNL, and the Minerals, Metals, and Materials Society (TMS) for the US

Department of Energy, suggests the following cost performance targets for key utility applications, and identify cost targets for flow batteries of $250/kWh in capital costs in 2015, decreasing to $100/kWh by 2030 [14]. Current estimates of costs for conventional batteries and flow batteries are significantly higher than the required targets: a 2008 estimate of RFB costs suggested nearly $2500/kW, albeit without specification of duration or sizing [15]. Regardless of detail, however, significant cost reduction must be achieved: technological improvements, material development, and economies of scale must be achieved to ensure success in the marketplace.

Table 1. Key performance targets for grid-storage applications, from Reference [14]

Application	Purpose	Key Performance Targets
Area and Frequency Regulation (Short Duration)	Reconciles momentary differences between supply and demand within a given area	Service Cost: $20 per MW Roundtrip Efficiency: 85%–90% System Lifetime: 10 years Discharge Duration: 15 minutes–2 hours Response Time: milliseconds
Renewables Grid Integration (Short Duration)	Offsets fluctuations of short-duration variation of renewables generation output Accommodates renewables generation at times of high grid congestion	Roundtrip Efficiency: 90% Cycle Life: 10 years Capacity: 1–20 MW Response Time: 1–2 seconds
Transmission and Distribution Upgrade Deferral (Long Duration)	Delays or avoids the need to upgrade transmission and/or distribution infrastructure Reduces loading on existing equipment to extend equipment life	Cost: $500 per kWh Discharge Duration: 2–4 hours Capacity: 1–100 MW Reliability: 99.9% System Life: 10 years
Load Following (Long Duration)	Changes power output in response to the changing balance between energy supply and demand Operates at partial load (i.e., increased output) without compromising performance or increasing emissions	Capital Cost: $1,500/kW or $500/kWh Operations and Maintenance Cost: $500/kWh Discharge Duration: 2–6 hours
Electric Energy Time Shift (Long Duration)	Stores inexpensive energy during low demand periods and discharges the energy during times of high demand (often referred to as arbitrage)	Capital Cost: $1,500/kW or $500/kWh Operations and Maintenance Cost: $250–$500/kWh Discharge Duration: 2–6 hours Efficiency: 70%–80% Response Time: 5–30 minutes

2. Redox-Flow-Battery Overview

RFBs can be classified by active species or solvent (aqueous and non-aqueous, respectively). Fig. 1 shows a generic RFB system. In the discharge mode, an anolyte solution flows through a porous electrode and reacts to generate electrons, which flow through the external circuit. The charge-carrying species are then transported to a separator (typically an ion-exchange membrane), which serves to separate the anolyte and catholyte solutions. The general reactions can be written as

$$\mathrm{A}^{n+} + x\mathrm{e}^- \xrightarrow{\text{charge}} \mathrm{A}^{(n-x)+} \quad \text{and} \quad \mathrm{A}^{(n-x)+} \xrightarrow{\text{discharge}} \mathrm{A}^{n+} + x\mathrm{e}^- \quad (\mathrm{n>x}) \tag{1}$$

and

$$\mathrm{B}^{m+} - y\mathrm{e}^- \xrightarrow{\text{charge}} \mathrm{B}^{(m+y)+} \quad \text{and} \quad \mathrm{B}^{(m+y)+} \xrightarrow{\text{discharge}} \mathrm{B}^{m+} - y\mathrm{e}^- \tag{2}$$

for the anode (negative electrode) and cathode (positive electrode), respectively.

The key transport mechanisms are shown in Fig. 1 for this generic system. The dominant losses in these systems, other than charge-transfer reaction kinetics, are related to the charge and mass transport in the electrolyte and separator, which are each discussed in turn in later sections of this review. Additionally, a key factor in many of these systems is crossover of species through the separator, which is dependent on current and membrane permeability. A sample RFB cell performance is shown in Fig. 2, where the charge and discharge are at different rates or current densities. One can see that similar to a fuel-cell polarization curve, there can be ohmic, mass-transport, and/or kinetic losses. The first part of the curves is dominated by kinetic overpotential, especially on charge. The middle part of the curves is dominated by ohmic or ionic-conduction losses, and the last part of the curves is typically a signature of reactant mass-transport limitations.

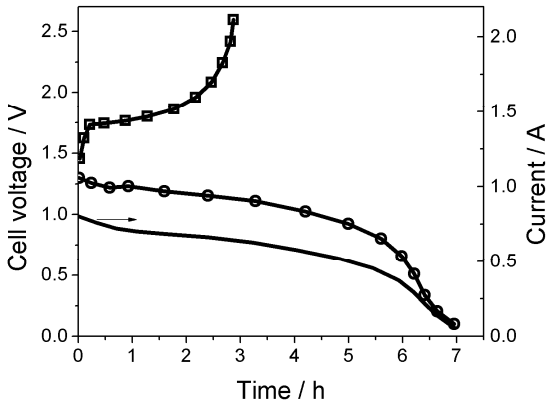

Fig. 2. Charge-discharge curves of an all vanadium RFB using 0.5 M $VOSO_4$ in 2 M H_2SO_4 and sulfonated polyethylene membrane. Electrode area= 90 cm^2; charging current density = 15 mA cm^{-2}; The discharge process is used a 1Ω resistor and the average discharge current density = 6 mA cm^{-2}. Adapted from Ref. [16] with permission.

The reactor in Fig. 1 consists of a stack of individual cells, where each cell contains the sites where electrochemical charge-transfer reactions occur as electrolyte flows through them, as well as a separator (either an electrolyte-filled gap or a selective membrane) to force the electrons through the external circuit. The arrangement of a typical cell is shown in Fig. 3, and individual cells can be arranged in series to increase the overall stack voltage. Generally, stacks are arranged in a bipolar fashion so that current flows in series from one cell to the next.

One of the key attributes of RFBs that suggests significant promise for stationary applications is the fact that, for many configurations, there is no physical transfer of material across the electrode/electrolyte interface. While there are some configurations that can be categorized as flow batteries only in the sense that the active material flows from outside of the cell to the electrode surface, most flow-battery systems under development utilize reversible solution-phase electrochemical couples on two electrodes to store chemical energy. Instead of storing the electrochemical reactants within the electrode itself, as with metal/metal alloy or intercalation electrodes, the reactants are dissolved in electrolytic solutions and stored in external

tanks. Both the oxidized and reduced form of each reactant are soluble in the electrolyte, so they can be carried to/from the electrode surface in the same phase. Only the relative concentrations of oxidized and reduced forms change in each stream over the course of charge and discharge.

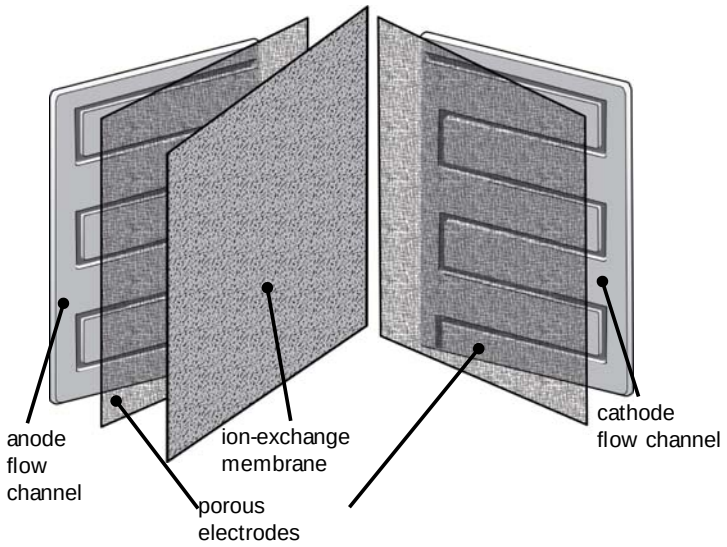

Fig. 3. Schematic diagram of standard RFB cell construction.

The electrodes in most RFB configurations are not required to undergo physical changes such as phase change or insertion/deinsertion during operation, because the changes are occurring in the dissolved reactants in the solution phase adjacent to the solid-electrode surfaces. Though there are exceptions to this formulation, as mentioned in the next section, this feature generally affords the opportunity to simplify the electrode design considerably. As a consequence of the charge-transfer characteristics, the cycle life of a RFB is not directly influenced by depth-of-discharge or number of cycles the way that conventional rechargeable batteries are. Side reactions can, of course, complicate design and operation, but if the reactions proceed as intended, degradation of the electrode surface need not proceed as a matter of course.

The decoupling of storage and reaction in RFB systems is an advantage in terms of flexibility, but it complicates their designs relative to conventional batteries, and adds a mechanical balance-of-plant element for pumping the often highly corrosive liquid electrolyte; as a result, their specific mass and volumetric energy densities are much lower than conventional batteries. A RFB configuration can nevertheless exceed the performance of other grid-storage technologies and does not require specific geographical siting, as pumped hydroelectric and compressed-air energy storage (CAES) do.

Additionally, RFBs offer the important advantage that power and energy outputs are independent variables since the power is determined by the reactor size and the amount of energy stored depends on the reactants chosen, their concentration, and the size of the reactant tanks [16-18]. The amount of energy that can be stored in a conventional sealed battery is generally limited by the effective path lengths for diffusion and migration in the direction normal to the current collector; making an electrode thicker will add to the amount of active material, but one experiences diminishing returns in terms of energy extraction because of diffusional and ohmic losses in these systems.

As shown in Fig. 1, most RFB systems currently require two separate electrolyte tanks: one for the anolyte and another for the catholyte. This ensures that the potentials at each electrode are close to the reversible potential for each of the half-cell reactions, and side reactions or competition from the other half-cell reactions are minimized. This does, however, add to the size and cost of the system, and it also requires a uniform delivery of the dissolved species to the entire surface area as oftentimes most of the convective flow is parallel to the electrode surface, rather than being flowed directly through it. Details of ion transport and flow configurations are discussed more thoroughly in a subsequent section.

The key costs of RFBs are the active material stored in the electrolyte and the electrochemical cell itself. The construction costs of the cell scale with the total power requirement of the application, but these costs are directly rated to the specific power of the device itself, i.e., how effectively the materials are utilized. While RFBs ought to be able to operate at relatively high current densities, as convection can be employed to deliver reactants to the electrode surface, RFBs have typically been operated at current densities consistent with conventional batteries without convection. It is anticipated that electrolyte management and cell design can deliver significant improvements in power density, thereby reducing considerably cell material costs.

2.1 Redox-flow-battery chemistries

Several battery technologies have been considered for grid-based storage in recent decades. Traditional rechargeable batteries have been modified and optimized for grid-based storage and are being deployed in some installations, including lead-acid, nickel-based, and lithium-ion batteries but we turn our attention to RFBs, which have been demonstrated on the order of 100 kW to 10 MW. RFBs are generally categorized based upon the anolyte and catholyte that comprise the form of energy storage of the system. Fig. 4 shows the basic redox couples, charge-transfer, and ion carrier migration modes in various specific RFBs. As shown in Fig. 4, configurations with the same species, *i*, but different oxidation states (such as all-vanadium) as well as different active species in the anolyte and catholyte are used. In this section, we introduce the various important RFB types and briefly some of the advantages, disadvantages, and challenges of each.

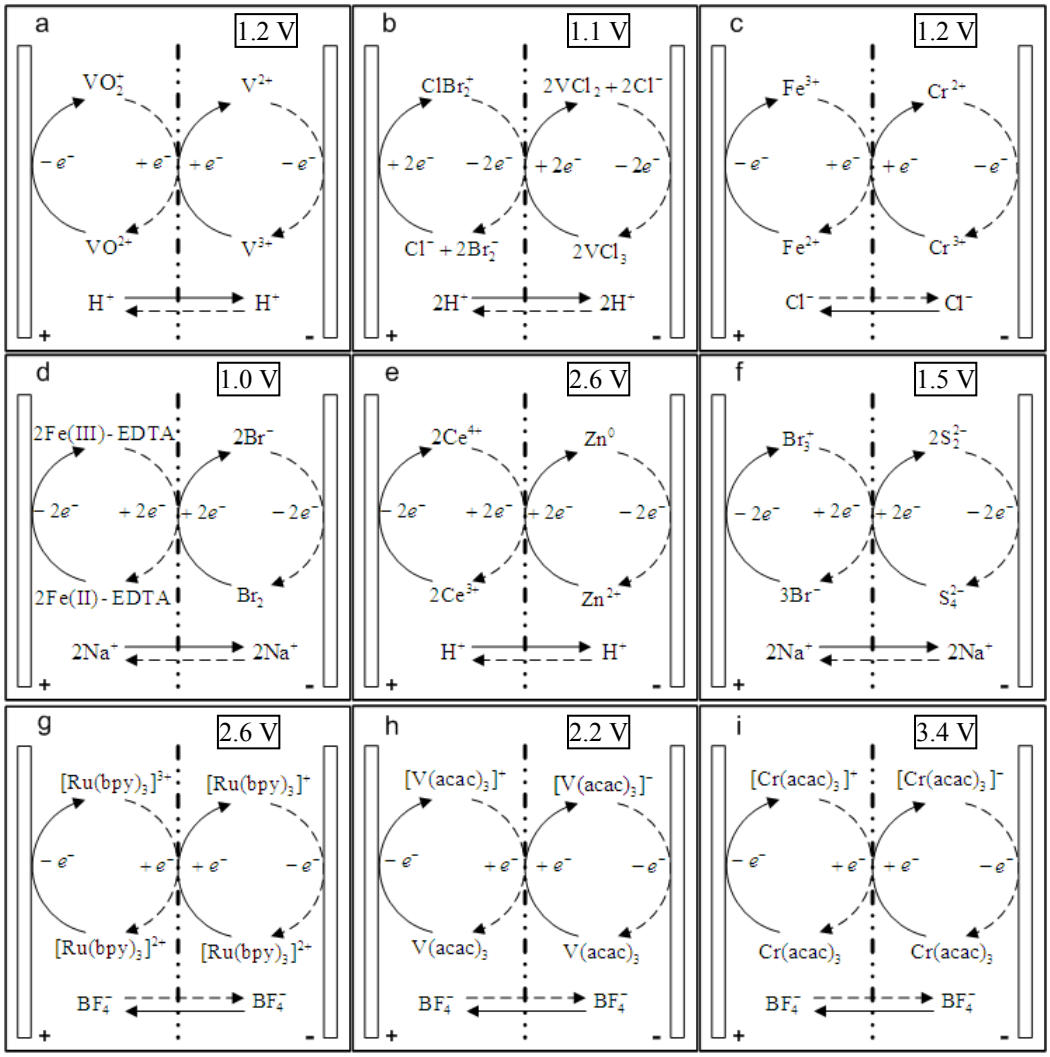

Fig. 4. Schematic of charge transport in various redox-flow systems (the values give the potential of the redox couple). (a) all vanadium, (b) vanadium/bromine, (c) iron/chromium, (d) Fe-EDTA/bromine, (e) Zinc/cerium, (f) bromine/polysulphide, (g) nonaqueous ruthenium/bpyridine, (h) nonaqueous vanadium/acetylacetonate, (i) nonaqueous chromium/acetylacetonate.

2.1.1 Iron/chromium

Modern development of what we might term a RFB began with the development of an iron/chromium system (Fe/Cr) in the 1970s at NASA, which demonstrated a 1 kW/13 kWh system for a photovoltaic-array application [19, 20]. The Fe/Cr system is based upon an aqueous solution of a ferric/ferrous redox couple at the positive electrode (Fe^{2+}/Fe^{3+}); the negative electrolyte is a mixture of chromic and chromous ions (Cr^{2+}/Cr^{3+}); most systems use

hydrochloric acid as the supporting electrolyte. The charge-transfer reactions at each electrode are

$$Fe^{2+} \leftrightharpoons Fe^{3+} + e^{-}, E^{0} = 0.77\text{V vs. RHE} \quad (3)$$

and

$$Cr^{2+} \leftrightharpoons Cr^{3+} + e^{-}, E^{0} = -0.41\text{ V } vs.\text{ RHE} \quad (4)$$

The system can operate with an ion-exchange membrane/separator and low-cost carbon-felt electrodes. Both charge-transfer reactions require only a single-electron transfer, which is expected to simplify charge transfer and result in reasonable surface overpotentials without specific electrocatalysts. Indeed, the iron redox couple is highly reversible on carbon or graphite electrodes, but the chromium redox couple has significantly slower kinetics, and does require electrocatalysts. This system has a relatively low open-circuit potential (between 0.90 and 1.20 V), and designers must endure crossover of iron to the chromium stream and vice-versa. Some Japanese companies built similar batteries by licensing the NASA patents, but have not shown improvement in the low output voltage and efficiency [21].

2.1.2 Bromine/polysulfide

The bromine/polysulphide RFB was patented by Remick in 1984 [17] then extensively studied by Regenesys Technology [22] from 1993 until 2006 when it was acquired by VRB Power Systems [5]. To date, three series of bromine/polysulphide RFB systems have been developed, including 5, 20, and 100 kW class systems. A commercial-size 15 MW system was successfully demonstrated. This plant used up to 120 modules, and 200 bipolar electrodes with an energy storage capacity up to 12 MWh and two 1800 m^3 electrolyte storage tanks [23].

In the bromine/polysulfide system, the positive electrolyte is sodium bromide, and the negative electrolyte is sodium polysulfide, though, the counter-ion could be replaced with another cation. The key attributes of this system are that the species that comprise the two electrolytes are abundant and reasonably inexpensive; furthermore, they are highly soluble in aqueous electrolytes, which reduces the volume of electrolyte that is required to store a given quantity of charge. At the positive electrode, three bromide ions combine to form the tribromide ion

$$3\mathrm{Br}^- \leftrightharpoons \mathrm{Br}_3^- + 2e^-,\ E^0 = 1.09\mathrm{V}\ vs.\ \mathrm{RHE} \tag{5}$$

At the negative electrode, the sulfur in solution is shuttled between polysulfide and sulfide

$$2\mathrm{S}_2^{2-} \leftrightharpoons \mathrm{S}_4^{2-} + 2e^-,\ E^0 = -0.265\mathrm{V}\ vs.\ \mathrm{RHE} \tag{6}$$

In this system, all of the electroactive species are anions, so a cation-exchange membrane is needed to prevent mixing of the anolyte and catholyte streams. Charge is carried via sodium ions through the membrane. When activated carbon/polyolefin composite electrodes were used in this system, the voltage increased from 1.7 V to 2.1 V during the charging process due to adsorption of bromine in the activated carbon [24]. This system is prone to crossover and mixing of the electrolytes, however, which can lead to precipitation of sulfur species and the formation of H_2S and Br_2.

2.1.3 All-vanadium

In both of the systems described above, a chief concern and liability is the incompatibility between, and sensitivity of, the two electrolyte streams to contamination from the other. If a species crosses over and reacts irreversibly with elements in the opposite stream, it comprises not just an efficiency loss on that particular charge/discharge cycle, but a loss of capacity and

degradation in the overall performance of the system, which may result in expensive electrolyte separation and reactant recovery. To this end, it is helpful to develop a system with more than two oxidation states of the same element, wherein crossover only represents an efficiency loss as no species are irreversibly consumed or removed from their reactive electrolytic solution. The all-vanadium system employs the V (II)/V(III) redox couple at the negative electrode and the V(IV)/V(V) redox couple at the positive electrode, generally identified to exist in the form of VO^{2+} and VO_2^+

$$V^{2+} \leftrightharpoons V^{3+} + e^-,\ E^0 = -0.26\text{V } vs.\text{ RHE} \tag{7}$$

$$\text{VO}^{2+} + \text{H}_2\text{O} \leftrightharpoons \text{VO}_2^+ + 2\text{H}^+ + e^-,\ E^0 = 1.00\text{V } vs.\text{ RHE} \tag{8}$$

In this case, the current is maintained by the migration of protons across the membrane separator. While it is nominally the change in the oxidation state of vanadium on either side of the membrane that stores and releases charge, there is a change in the pH of the solution over the course of a charge and discharge cycle. While crossover of the different oxidation states of vanadium comprises an efficiency loss, the proper forms can be regenerated electrochemically, which eases the stringency of maintenance requirements.

While exploratory research on vanadium as a redox couple began at NASA [8], the all-vanadium redox battery (VRB) was invented and developed by Maria Skyllas-Kazacos and her co-workers at the University of New South Wales [16, 25, 26]. Research has continued on this technology since that time. As a promising technology for storing intermittent renewable energy, VRB systems have received perhaps the most attention of all RFBs [16, 27-39]. In fact, prototypes up to the range of MW in power and MWh in energy-storage capacity have been

demonstrated [3, 35, 40-47]. Fig. 5 shows the 5 to 10 kW VRB stack developed by Skyllas-Kazacos' group along with its general efficiencies.

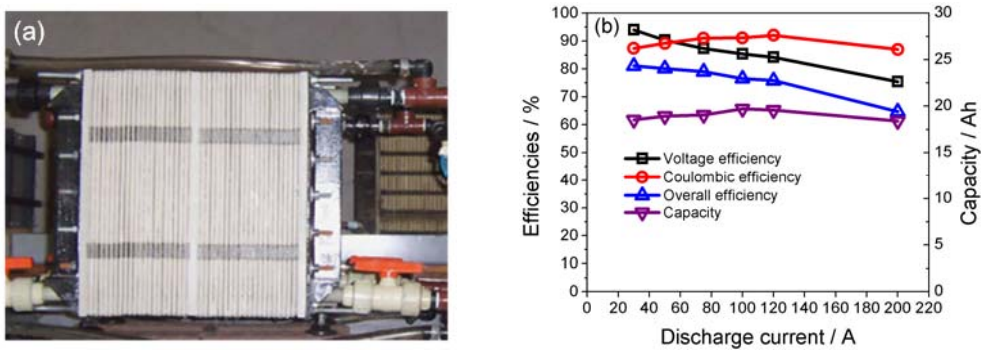

Fig. 5. (a) 5–10 kW VRB stack. (b) Stack efficiencies and capacity *vs.* stack discharge current. Adapted from Ref. [48] with permission.

While energy density is not necessarily a primary concern for stationary, grid applications, nonetheless, the VRB energy density is limited by the solubility of vanadium in the electrolyte stream and precipitation can occur; the solubility limits depend upon both acid concentration and temperature [49].

2.1.4 Vanadium/bromine

Because there are limits to how much vanadium can be stored in solution in the VRB system, some of the same researchers who pioneered the work on the VRB cell noted that vanadium solubility could be boosted in the presence of halide ions. In this case, during charging the bromide ions in the positive half-cell undergo oxidation to what is assumed to be the polyhalide ion Br_2Cl^-; the formal potential of this couple is about 1.3 V more positive than the V(II)/V(III) couple [48, 50, 51]. The researchers were able to show significantly higher solubilities in this system: vanadium-bromide solutions with nearly twice the solubility on a molar basis relative to vanadium sulfate solutions were demonstrated. The higher solubility of vanadium bromine results in higher energy densities (35 to 70 Wh/L) compared to the VRB

systems (25 to 35 Wh/L). However, the potential concern of vanadium/bromine redox systems is toxic bromine-vapor emissions during operation, and thus Skyllas-Kazacos also used bromine complexing agents including tetrabutylammonium bromine, polyethylene glycol, N-methyl-N-ethyl morpholinium bromide, and N-methyl-N-ethyl pyrrolidinium bromide to decrease or eliminate bromine-vapor emissions during operation [38]. Shown in Fig. 6 is a typical series of charge-discharge curves using a charge-discharge current density of 20 mA/cm^2 [48]. Generally, the coulombic efficiency increases with increasing current density due to lower self-discharge through the membrane; however, it decreases as temperature increases due to more rapid diffusion of vanadium and polybromide ions through the membrane.

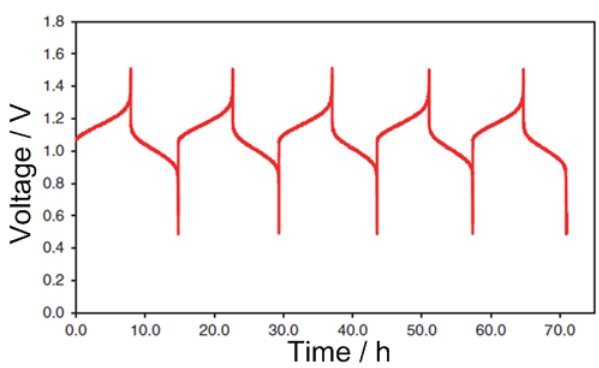

Fig. 6. A series of charge-discharge curves for vanadium-bromine redox cells using 2.5 M vanadium bromide electrolyte with the charge-discharge current density = 20 mA cm^{-2} and T=30 ^{o}C. Adapted from Ref. [48] with permission. These curves do not correspond to the same stack operating conditions as shown in Fig. 5.

2.1.5 Hydrogen-based systems

A fuel cell takes a fuel (normally hydrogen) and an oxidant (typically air) and produces electricity and water. For a fuel cell, hydrogen oxidizes at the anode according to the reaction

$$H_2 \rightarrow 2H^+ + 2e^- \text{ , } E^0 = 0 \text{ V vs RHE} \qquad (9)$$

and, at the cathode, oxygen is reduced

$$4H^+ + 4e^- + O_2 \rightarrow 2H_2O, E^0 = 1.229 \text{ V vs RHE} \quad (10)$$

If one were to design a system where the fuel cell acts in both the charge and discharge directions (i.e., a reversible or regenerative fuel cell), then a RFB system would exist. Such a RFB system has been examined both with the same and different stacks for charge and discharge [52-55]. This system is inherently different from the RFBs discussed above since the reactants are in the gas and not liquid phase, which enhances mass transfer at the expense of storage tank volume, and thus hydrogen compression or novel hydrogen-storage materials are is needed. Although mass transfer is typically rapid, the oxygen reactions are known to be very sluggish and result in very large overpotentials [56], thereby rendering the overall efficiency of the system to be relatively low. To enhance as well as drive down the cost of the hydrogen/oxygen system, strategies including looking at alkaline media, high temperatures, and closed systems with oxygen and not air. Also, because of the difficulty associated with finding robust and effective oxygen reduction/evolution catalysts, different oxidants have been examined including bromine and chlorine, both of which react rapidly on carbon surfaces [57-59].

2.1.6 Hybrid redox-flow batteries

There are other battery configurations that share a development heritage and some common issues with what we would classify as RFBs in that the active material can be introduced to, or removed from, the electrochemical cell without disassembling the cell structure, but which do not store all of the active material in a liquid or gaseous form per se. As such, we might consider them semi-flow cells with electrochemical reactions that are more complicated than simply shuttling between the oxidation states of a single species.

2.1.6.1 Zinc/bromine

The prototypical hybrid or semi-flow RFB is the zinc/bromine system [60]. In this system, electrolyte solutions containing the reactive species are stored in external tanks and circulated through each cell in the stack, but the zinc reaction does not only involve dissolved species in the aqueous phase. At the positive electrode, bromide ions are transformed to bromine and back, see equation 5. It is important to note that the bromide ions can combine with bromine molecules to generate the tribromide ion [61]

$$Br_2 + Br^- \leftrightharpoons Br_3^- \tag{11}$$

which occurs primarily in liquid bromine. In this system, relatively high concentrations of Br^- and Br_2 can be utilized, enhancing both reaction kinetics and energy density. The toxicity of Br_2 and the highly complexing/corroding character of concentrated HBr are limitations however. The toxicity of Br_2 can be mitigated by the use of complexing agents [62], but the effect of complexing agents on kinetics has not been studied quantitatively, particularly in strongly acidic supporting electrolyte.

At the negative electrode, zinc metal is dissolved and redeposited,

$$Zn \leftrightharpoons Zn^{2+} + 2e^-,\ E^0 = -\ 0.76\text{V}\ vs.\ \text{RHE} \tag{12}$$

To prevent self-discharge by combination of zinc and bromine, separate flowing streams of aqueous zinc bromide and bromine circulate in separate loops, separated by an ion-exchange membrane or a microporous film [63].

The metal negative electrode allows for a compact electrode, thus increasing the energy density. In addition, the zinc/bromine system has a high cell voltage, good reversibility, and expectations of low material costs. However, the demonstration of zinc/bromine has been limited

due to material corrosion, dendrite formation and electrical shorting, high self-discharge rates, low energy efficiencies, and short cycle life. RedFlow Ltd. successfully demonstrated a zinc/bromine RFB unit up to MW size with an energy efficiency of nearly 74 % in Australia [64]. The cell architecture was designed to optimize plating and de-plating efficiency of zinc during charging and discharging operations. Derivatives of the zinc/bromine system include other halogens such as zinc/chlorine, which typically have similar performance and issues [65].

2.1.6.2 Soluble lead acid

A soluble form of the lead-acid battery has also been considered [66]. The charge-transfer reactions as written are the same as in a traditional sealed lead-acid battery configuration. Lead-acid batteries do not shuttle the same ion between the negative and positive electrode; that is, Pb^{2+} is introduced and removed from solution at the negative electrode as lead is dissolved and plated,

$$\mathrm{Pb} \leftrightharpoons \mathrm{Pb}^{2+} + 2e^{-},\ E^{0} = -\ 0.13\ vs.\ \mathrm{RHE} \tag{13}$$

but at the positive electrode, lead ions combine with water to produce lead dioxide and protons,

$$\mathrm{Pb}^{2+} + 2\mathrm{H}_2\mathrm{O} \leftrightharpoons \mathrm{PbO}_2 + 4\mathrm{H}^{+} + 2e^{-}, E^{0} = 1.49V\ vs.\ \mathrm{RHE} \tag{14}$$

As lead ions are produced in the oxidation step at the negative electrode and produced in the reduction step at the positive electrode on discharge, there is not a risk of crossover lowering the overall efficiency of the system. As long as the solid forms of lead and lead dioxide are maintained at the negative and positive electrodes, circulation of electrolyte can maintain the open-circuit potential of the battery and allow greater specific cell performance than with sealed or flooded lead-acid cells, assuming minimal weight and volume of the external storage tank. As

with other semi-solid flow configurations, there are risks associated with maintaining the morphology of the solid phase as material can detach or grow across the separator gap to cause short-circuit problems.

2.1.6.3 All iron

Similar to the all-vanadium RFB, the all-iron system [67, 68] involves only a single element, where on one electrode iron(II) goes to iron(III), equation 3, and on the other plating of iron occurs

$$\mathrm{Fe} \Leftrightarrow \mathrm{Fe}^{2+} + 2e^{-}, E^{0} = -0.3\mathrm{V\ vs.\ RHE} \tag{15}$$

Due to the single species, crossover is not as much a concern although it is still a current inefficiency. This system has some of the same issues as the other hybrid batteries including getting uniform plating of the metal, thereby necessitating precise pH control and supporting electrolyte; however, iron does not have the extensive dendrite problems of zinc. The benefits of the cell are also that the materials are non hazardous and inexpensive. These are balanced by the fact that the overall cell voltage is relatively low and hydrogen generation can occur, although iron is a poor hydrogen-evolution catalyst.

2.2.7 Non-aqueous redox-flow batteries

The use of non-aqueous electrolytes in RFB configurations has been considered because of the higher cell potentials that are possible when one is not concerned by the breakdown of the aqueous electrolyte. In addition, many couples and reactants are much more soluble in non-aqueous solvents. However, the challenges of low electrolyte conductivities, stability, and cost limit the development of non-aqueous RFB systems.

As an example, the zinc/cerium cell has been worked on by Plurion Limited. As with the zinc/bromine cell, the negative electrode dissolves and plates zinc, equation 12, and at the positive electrode, cerium is shuttled between Ce(III) and Ce(IV)

$$Ce^{3+} \Leftrightarrow Ce^{4+} + e^{-}, E^{0} = 1.75\text{V vs. RHE} \quad (16)$$

The developers claim a cell potential of approximately 2.5 V on charging, but it drops below 2 V during discharge with an energy density of 37.5 to 120 Wh/L [69, 70]. The high operating potential window is achieved by using methane sulfonic acid rather than water as the solvent, thus avoiding decomposition of water into hydrogen and oxygen, as well as aiding in zinc plating. The redox reaction of Ce(III)/Ce(IV) is kinetically slow and Ce(III) has a somewhat low diffusivity [71, 72]. High acid strength facilitates the solubility of Ce(IV); however, the solubility of Ce(III) decreases at higher acid concentrations. Other electrochemical couples including zinc/chlorine [73], zinc/ferricyanide [70], and vanadium/cerium [74] have been considered. While non-aqueous electrolytes generally imply higher costs than aqueous electrolytes and must be vetted for environmental and chemical compatibility, the expansion of the operating potential window is attractive, as the cell potential difference has a direct impact on the amount of power that can be delivered for a specified current density.

Other examples of nonaqueous RFBs include that of Matsuda *et al*. [75] who demonstrated a redox system based on $[Ru(bpy)_3]^{2+}/[Ru(bpy)_3]^{3+}$ (bpy is bipyridine) as the anolyte and $[Ru(bpy)_3]^{+}/[Ru(bpy)_3]^{2+}$ as the catholyte in acetonitrile (CH_3CN) with tetraethylammonium tetrafluoroborate ($TEABF_4$) as the supporting electrolyte. This system yielded an open-circuit potential of 2.6 V, with an energy efficiency of 40 %. Chakrabarti *et al*. evaluated a redox system based on a ruthernium acetylacetonate, obtaining a cell potential of 1.77 V [76]. Yamamura *et*

al.[77] studied a non-aqueous system which used various uranium beta-diketonates with the cell potentials of about 1 V.

Recently, Thompson and co-workers demonstrated a redox-flow system using $M(acac)_3$ (M=V, Cr or Mn, and acac is acetylacetonate) with at least three different oxidation states [78-80]. The vanadium and chromium acetylacetonate systems showed higher open-circuit potentials, 2.2 and 3.4 V, respectively, compared to around 1.26 V for the aqueous VRB system. However, crossover and ohmic losses due to the large distances between positive and negative electrodes limited the coulombic efficiency. Although the $Mn(acac)_3$ system shows a lower open-circuit potential (1.1 V) than that of $V(acac)_3$, $Cr(acac)_3$, and VRB, it exhibits better reversibility both for Mn(II)/Mn(III) and Mn(III)/Mn(IV) redox couples, with a columbic efficiency approaching 97 % in a static H-type cell. Shinkle *et al*. studied the degradation mechanisms in the non-aqueous $V(acac)_3$ redox systems [81], and showed that environmental oxygen and water are associated with side reactions that affect the long-term charge-discharge response of the battery.

2.2.8 Other configurations

There is recent interest in the development of the lithium-air battery, which operates with a static lithium negative electrode, as might be found in a lithium-ion or lithium-polymer battery. Lithium ions combine with oxygen from air to form lithium oxide at the positive electrode on discharge; oxygen is regenerated during charging. Kraytsberg and Ein-Eli provide an overview of the technology [82]. There are many challenges with such a battery system, such as ensuring proper isolation of the negative electrode from oxygen and water crossover and ensuring an electrode structure that provides for facile oxygen transport and reversible oxide formation and

stripping. However, the promise for high energy density and low material costs suggest tremendous research opportunities.

Another recent flow-cell concept was invented by Yet-Ming Chiang's group at MIT and described by Duduta *et al*.[83, 84]. They proposed using typical intercalation electrode materials as active materials for a lithium rechargeable battery, but providing the active material in a slurry that can be mechanically pumped into and out of a reaction chamber. In the paper describing the concept, they note that they will be able to store much higher concentrations of active material in the solid component of the slurry than can be stored as ions dissolved in electrolyte (up to 24 M), thereby increasing the energy density well beyond what could be achieved in traditional RFBs.

3. Kinetics of Redox Reactions

The study of the kinetics of redox reactions occupies a central place in fundamental electrochemistry. Most of important concepts in the theory of electrode reactions were developed from the consideration of redox reactions. The simplest form of a redox reaction is a one-electron transfer of an electron to or from an electrode to an ion in solution, written generally as

$$O + ne^- \leftrightharpoons R \tag{17}$$

where O is the oxidized state and R the reduced state of the ion. In the simplest type of redox reaction, there are no changes in the ion other than the valence state and relaxation of the solvent around the ion. The prototypical example of such a reaction is the ferrous/ferric reaction in solutions of sulfuric acid (meticulously free of chloride ion, as discussed in more detail below). The reactions become more complex, and the theory more involved, when the ions are complexed with neutral or other anions that do not participate in the electron transfer directly (i.e., it does not change valence or state of charge), but are part of the relaxation of solvating

ligands or assist the transfer of the electron from the electrode surface, termed mediated electron transfer. Ferri-/ferrocyanide and ferric/ferrous chloride would be examples, respectively, of such redox couples. There are also reactions involving multi-atom ions and reactions where one state is a neutral molecule that are termed redox reactions. There are no hard criteria for what is or is not a "redox" reaction, but a common feature is that it involves electron transfer that is at least measurably reversible. For the purposes here, we will discuss only the more well-studied reactions that have some promise as RFB couples as mentioned above.

Most of the fundamental principles for the kinetics of electron transfer can be found in two classic texts in electrochemistry, and those form the basis of the principles reviewed here. The first is the text by Vetter [85], which contains an interesting and unique description of the history of the development of the fundamental theory of electrode kinetics, including the familiar names of Butler and Volmer, but less recognized (in this context) names such as Gurney, Erdey-Gruz and Vetter himself [85]. This text also reviews experimental results for more than twenty-five redox couples, all from original papers published before *ca*. 1960, but these references remain in some cases as the best source of quantitative kinetic parameters versus more recent but qualitative (or less rigorous) measurements. Another important resource is the text by Bard and Faulkner [86], more accessible than the Vetter text, with notation and terminology that is more contemporary. Following the notation in Bard and Faulkner, the Butler-Volmer model of the kinetics of reaction produces the essential current (i) – overpotential (η) relationship as

$$i = i_0\left[\left(\frac{c_O(0,t)}{c_O^*}\right)\exp\left(\frac{\alpha F}{RT}\eta\right) - \left(\frac{c_R(0,t)}{c_R^*}\right)\exp\left(-\frac{(1-\alpha)F}{RT}\eta\right)\right] \tag{18}$$

where η is the overpotential, defined as the difference between the electrode potential under current flow and the rest (zero current) potential

$$\eta = \Phi_k - \Phi_p - E_{eq} \tag{19}$$

where Φ_k is the potential in phase k, and E_{eq} is the Nernst potential, which is related to the concentrations of the oxidized (c_O^*) and reduced (c_R^*) species by

$$E_{eq} = E^0 + \frac{RT}{F}\ln\left(\frac{c_O^*}{c_R^*}\right) \tag{20}$$

where i_o is the exchange current density, α is the transfer coefficient (or the symmetry factor in transition state theory), and R, T and F have their usual meaning. This form of the Butler-Volmer equation is important for both fundamental (experimental) kinetic studies and for modeling practical devices, since in both cases one needs to consider the contribution of mass transport of the ions from the bulk solution to the electrode surface.

The essential kinetic parameters determined experimentally are the exchange current density and the transfer coefficient. The exchange current is the magnitude of the partial anodic and cathodic currents which are equal at equilibrium, and are in turn related to the bulk concentrations by the standard rate constant, k^0,

$$i_0 = Fk^0 c_O^{*(1-\alpha)} c_R^{*\alpha} \tag{21}$$

Since the exchange current density varies with the concentration of the redox species, the more fundamental measure of kinetics for redox reactions is k^0. The grouped kinetic parameter i_0 is an important quantity to confirm experimentally. The transfer coefficient is usually measured from the slope of log i vs. η in the so-called Tafel region, where the back-reaction is negligible and the relationship between overpotential and current density reduces to

$$i = i_0\left(\frac{c_R(0,t)}{c_R^*}\right)\exp\left(\frac{(1-\alpha)F}{RT}\eta\right) \tag{22}$$

and the experimental current is either obtained under conditions where $c_R(0,t) = c_R^*$ or accurate mathematical correction can be made to the experimental value, for example, the solution of the convective-diffusion equation for the rotating-disk electrode [86]. Likewise, the value of i_0 can be obtained by extrapolation of the Tafel plot to $\eta = 0$. However, for fast kinetics, or where a second electrochemical reaction (e.g. hydrogen or oxygen evolution), occurs near the equilibrium potential, a linear Tafel plot may not be obtained and neither i_0 nor α may be obtained by this method. There are a number of other methods that may be used to obtain i_0 directly. In those cases, the concentration dependence of the exchange current density may be used to obtain α.

Following the pioneering theoretical framework introduced by Gerischer [87], modern quantum chemical theory of redox kinetics at electrode surfaces has focused on the distance of the redox ion from the electrode surface [88]. Modern theory typically distinguishes redox reactions as either "inner-sphere" or "outer-sphere", the latter referring to reactions where the redox ion is "inside" the plane of the inner Helmholtz ionic layer and the former "outside" [89]. Practically, this distinction is important in that inner-sphere reactions typically have a very large dependence of the reaction kinetics on the electrode material, in many cases by orders of magnitude; the hydrogen electrode is perhaps the most dramatic in this respect. For outer-sphere reactions, the kinetic effect of different electrode materials is much less, but not insignificant. However, this distinction in electrode-material dependence is not essential, and there are examples where inner-sphere reactions have a relatively small dependence on the electrode material, e.g. the Br_2/Br^- reaction. The detailed discussion of the effect of electrode materials on the kinetics is beyond the scope of this review.

One can estimate the rough order of magnitude that the kinetic rate must be for a practical RFB. For example, using some of the metrics in Table 1 (i.e., a RFB must have high electrical

efficiency, e.g. at least 80 % round-trip, or 90 % in each direction) and assuming a typical cell voltage of 1.5 V, then the kinetic overpotential must be less than 150 mV throughout the charge/discharge cycle. Assuming a minimum practical current density of at least 50 mA/cm^2, a roughness factor of 10, i.e. 10 cm^2 surface per unit electrode geometric area, and a transfer coefficient of 0.5, the exchange current density must be greater than 0.3 mA/cm^2 (real) throughout the charge/discharge cycle. Assuming 1 M solutions at 50 % state of charge, and assuming 90 % utilization of the redox ions in the cycle, the minimum value of the standard rate constant k^0 is ca. 10^{-5} cm/s. If the rate constant is significantly less than this value, some compromises must be made to achieve a practical device which may increase cost and/or utility. For example, higher surface area/porosity electrodes will compromise a simple flow-by/through design. Reduced current density will reduce power density and result in larger electrodes and more material per unit volume in the RFB. The estimated value above can be compared to those in literature as shown in Table 2.

Table 2. Kinetic parameters for redox reactions used in flow batteries. Supporting electrolyte in most cases is 1 M H_2SO_4 or $HClO_4$; concentration of redox species is 10^{-3} to 10^{-2} M.

Redox couple	α	k^0(cm/s)	Electrode	Reference
Fe^{3+}/Fe^{2+}	0.59	2.2×10^{-5}	Au(poly)	[90]
	0.55	1.2×10^{-5}	Au(111)	[62]
Cr^{3+}/Cr^{2+}	~ 0.5	2×10^{-4}	Hg	[91]
VO_2^+/VO^{2+}	0.42	3.0×10^{-7}	Graphite	[92]
	0.3	$1–3 \times 10^{-6}$	Carbon	[93]
V^{3+}/V^{2+}	~ 0.5	4×10^{-3}	Hg	[91]
Ce^{4+}/Ce^{3+}	~ 0.5	1.6×10^{-3}	Pt	[85]
Br_2/Br^-	0.35	1.7×10^{-2}	Pt(poly)	[94]
	0.46	$5.8\times–10^{-4}$	Vitreous carbon	[95]

The results in Table 2 show that of all the redox couples recently or currently in use in practical RFBs, only the VO^{2+}/VO_2^+ couple has a clear kinetic limitation and, in fact, is clearly problematic. This is not surprising since this redox is not a simple one-electron transfer reaction, but is in modern terminology an oxygen transfer reaction as shown in equation 8. As discussed in detail recently by Gattrell *et al.* [92], this reaction is a multi-step reaction in which oxygen transfer (a chemical step) may precede or follow an electron-transfer step, denoted in modern terminology as a CE or EC mechanism. Such reactions usually have current-potential relations which differ significantly from the ideal Butler-Volmer form, and that is the case here. The kinetic data by Gattrell *et al.* were obtained using a graphite RDE, which should be directly applicable to practical cells which use carbon-felt electrodes. Although the quantitative data in Table 2 was obtained using a Hg electrode, the polarization curves shown for the V^{2+}/V^{3+} electrode with a graphite RDE in Gattrell *et al.* indicate a rate constant >> 10^{-5} cm/s.

The dependence of the VO^{2+}/VO_2^+ couple on electrode material has not been very well-studied. Skyllas-Kazacos and co-workers [93] reported somewhat larger exchange-current densities for less well-characterized "carbon" electrodes than Gattrell *et al*. and suggested it is possible to enhance kinetics by surface treatment of carbon-based electrodes. Zhong *et al*. fabricated conducting polyethylene (PE) composite electrodes with low resistivities by mixing polyethylene with conducting fillers (carbon black, graphite power and fiber) [93]. The chemical treatment of graphite fiber-based composite polymer electrodes with chromate-sulphuric acid was shown to enhance the surface and improve reactivity for the electrode reactions. Carbon-polypropylene (PP) composite electrodes modified with rubber show better mechanical properties, better impermeability and better overall conductivity compared to the PE composite electrodes [96]. A voltage efficiency as high as 91 % was obtained for the VRB with the carbon-

PP composite electrodes. Graphene oxide nanoplatelets (GONPs) demonstrated a more favorable electrocatalytic activity for V(V)/V(IV) and V(III)/V(II) redox couples than pristine graphite for the VRBs. It is found that the V(III)/V(II) redox reaction strongly depends on the formation of surface active functional groups of C-OH and COOH [97]. However, it is not clear that using an electrode material other than graphite/carbon would be cost effective.

In contemporary studies of heterogeneous electron transfer reactions, the Fe^{3+}/Fe^{2+} reaction is still considered to be the prototypical outer-sphere reaction amenable to quantitative quantum chemical treatment using modern ab-initio methods. The data shown in Table 2 are relatively recent measurements using sulfuric-acid solutions rigorously purified specifically of chloride ion (to ppb levels). Following the pioneering work by Nagy *et al*. [98], it is now widely recognized that with Pt and Au electrodes, the presence of even trace amounts of chloride ion enhances the experimental rate of electron transfer by at least two-orders of magnitude, probably by a mediated or bridging transfer of the electron via adsorbed chloride anions. While it has not been proven conclusively that the "chloride effect" is exclusive to Pt and Au, theoretical considerations are consistent with such an expectation, and qualitative data with carbon-felt electrodes suggest this is the case, and that the kinetic parameters given in Table 2 should be applicable to carbon electrodes in a practical battery.

The Ce^{4+}/Ce^{3+} was studied in detail by Vetter [85] including rigorous correction for the partial current from oxygen evolution. The reaction has not been the subject of many studies since then. The corrosion of the electrode material and the parasitic effect of oxygen evolution are serious issues for a practical device. Use of stable electrode materials such as IrO_2 evolve significant oxygen, thereby reducing efficiency and requiring active cell rebalancing and maintenance. Carbon electrodes will undergo significant corrosion and not have practical

lifetimes at these operating potentials [99]. Practical use of this redox couple in a RFB will require a scientific breakthrough in electrode material.

Like the VO^{2+}/VO_2^+ couple, the Br_2/Br^- is a multi-step reaction with at least one chemical step, that of breaking/making the Br-Br bond, either preceding or following electron transfer. The chemical step is, however, much simpler than the oxygen transfer step in the VO^{2+}/VO_2^+ reaction. The kinetics of this reaction are not nearly as dependent on electrode material as, for example, the hydrogen electrode, to which it is mechanistically similar [85]. The data for Pt and vitreous carbon shown in Table 2 illustrate this fact well, with the difference in rate constant being only a factor 30, whereas for the hydrogen electrode the difference would be several orders of magnitude. The reason for this difference can be explained rather easily qualitatively by considering the bond energies involved in the possible/probable chemical steps, for example, that of dissociating the Br_2 molecule to form an adsorbed state of Br, analogous to the Tafel step in the hydrogen electrode. The bond energy of Br_2 is 192 kJ/mol vs. 457 kJ/mol for H_2. To be energetically favorable, the adsorption energy of the Br needs to be greater than 86 kJ/mol vs. 228.5 kJ/mol for H. If one-electron transfer precedes dissociation, i.e. the dissociation is of a Br_2^- species, then the adsorption energy required is even less. Similar considerations apply in the anodic direction, where the proton is much more strongly solvated than the bromide ion (by about a factor of 3 [100]), meaning much weaker chemical interaction with the electrode is required for forming an adsorbed Br intermediate than an H intermediate. The shapes of the polarization curves on both Pt and vitreous carbon are very similar, differing primarily in the magnitude of the current scale, and on neither electrode material does one observe a classic Butler-Volmer relation. For the purposes of Table 2, only the reduction data was used to extract a

rate constant using the Tafel region. The authors of both papers propose the same reaction mechanism for both electrode materials,

$$\mathrm{Br}_2 + e^- \leftrightharpoons \mathrm{Br}_{ad} + \mathrm{Br}^- \tag{23}$$

and

$$\mathrm{Br}_{ad} + e^- \leftrightharpoons \mathrm{Br}^- \tag{24}$$

The first step above is not an elementary step, and electron transfer must either precede or follow dissociation. From the energetic considerations above, it seems reasonable to suggest that on carbon electrodes the electron transfer precedes dissociation, consistent with relatively weak adsorption of Br_{ad} on this surface. In many ways, the Br_2/Br^- couple is the ideal redox electrode for RFBs. The reaction is relatively facile, and the kinetics are not strongly dependent on electrode material, such that carbon/graphite electrodes provide reasonable performance, as demonstrated in zinc/bromine RFBs [60]. This material flexibility is a significant advantage in practical electrode design.

Before examining surface-area effects, a mention should be made about typical RFB electrode materials. As noted above, graphitic or vitreous carbon materials are widely used in RFBs [27, 28, 30, 101], such as graphite, carbon felt, carbon fiber, thermal and acid treated graphite, carbon-polymer composite materials, carbon nanotubes, Ir-modified carbon felt and graphene-oxide nanoplatelets. In general, RFB couples are chosen for the facile kinetics so highly active catalytic materials are not necessary. Nonetheless, it has been found that various surface treatments can lead to improved reaction kinetics on carbon electrodes. Chemical etching [102], thermal treatment [103], chemical doping [11], carbon nanotube addition [104], and addition of metallic catalyst sites to the carbon fibers [105] have all been attempted. Aside from catalytic activity, the main criteria for electrode materials are electrical conductivity, chemical

stability and durability in the reaction environment. Carbon and graphite materials meet both these requirements, though metal foams and meshes are also candidates [106, 107]. The search for improved electroactive materials for RFBs will no doubt continue to be actively pursued.

3.1 Active surface area

The above kinetic constants and equations (e.g,. equation 18) are for rates per unit catalyst area. As mentioned, one way to compensate for a slower reaction is to increase the roughness factor, a, or catalyst surface area per unit geometric area. For example, ignoring double-layer charging and assuming electroneutrality, one can write a current balance between ionic and electronic current,

$$\nabla \cdot \mathbf{i}_2 = -\nabla \cdot \mathbf{i}_1 = a_{1,2} i_{h,1-2} \tag{25}$$

where it is evident that the current generation source term is directly proportional to the specific interfacial area, $a_{1,2}$, which can be related to the roughness factor discussed above Table 2 by accounting for the thickness of the electrode. In the above equation, $-\nabla \cdot \mathbf{i}_1$ represents the total anodic rate of electrochemical reactions per unit volume of electrode and $i_{h,1-2}$ is the transfer current for reaction h between the ionic and electronic materials; for RFBs, the electronic current (1) is the electrons and the ionic current (2) are the reactive ion species. Thus, the surface area in the porous electrode is critical to RFB performance.

An optimum surface area in a porous medium is directly linked to the physical and transport properties of the medium, namely, porosity and permeability, respectively. From an electrochemical standpoint it is desirable to have the highest possible surface area, but this tends to conflict with the need to minimize pressure drop and pumping costs, which favor high permeability. A brief analysis of the interplay between these two key parameters follows.

Typical RFB carbon-fiber-paper or carbon-felt electrode materials have a porosity around 0.8, a fiber diameter of approximately 10 μm and a permeability of 20×10^{-8} cm^2. A qualitative estimate of the surface area variation with fiber diameter can be obtained using a filament analogue model which simply involves finding the number of cylinders N of a given diameter d_f that give a specified porosity ε (cm^3/cm^3), then determining the specific surface area $a_{1,2}$ (cm^2/cm^3) of N cylinders. A simple formula for this relationship is given by Carta *et al.* [108]

$$a_{1,2} = \frac{4(1-\varepsilon)}{d_f} \tag{26}$$

Figure 7 shows the variation of total surface area as a function of fiber diameter for an 80 % porous material. The actual surface area in a real fiber bed may be less than this value since fibers contact and overlap each other, or more if the fibers are not truly cylindrical but rough or ridged. In terms of a roughness factor, using a typical felt properties and a thickness of a few millimeters, a value of around 50 is obtained. Also shown in Fig. 7 is the absolute-permeability change expected as calculated from the Carman-Kozeny equation [109], which has been shown to adequately describe the variation of permeability with porosity due to compression in fibrous materials [110] and is assumed to apply here.

Clearly, the fiber diameter dramatically impacts both aspects and unfortunately in opposing directions. Increasing the fiber diameter from 10 to 100 μm improves the permeability by a factor of 100, but reduces the surface area by a factor of 10. The same general trend would be true for other random electrodes such as particulate beds. Efforts to increase active surface area in a flowing electrolyte by using particles with microporosity have been reported [18], but, not surprisingly, this additional surface area does not contribute significantly to the electrochemically active area since such internal surfaces are highly diffusion limited.

Attempts to increase the roughness of the electrode surface could be beneficial, but typically it is more profitable to modify the surface for increased kinetic or catalytic behavior rather than just surface area.

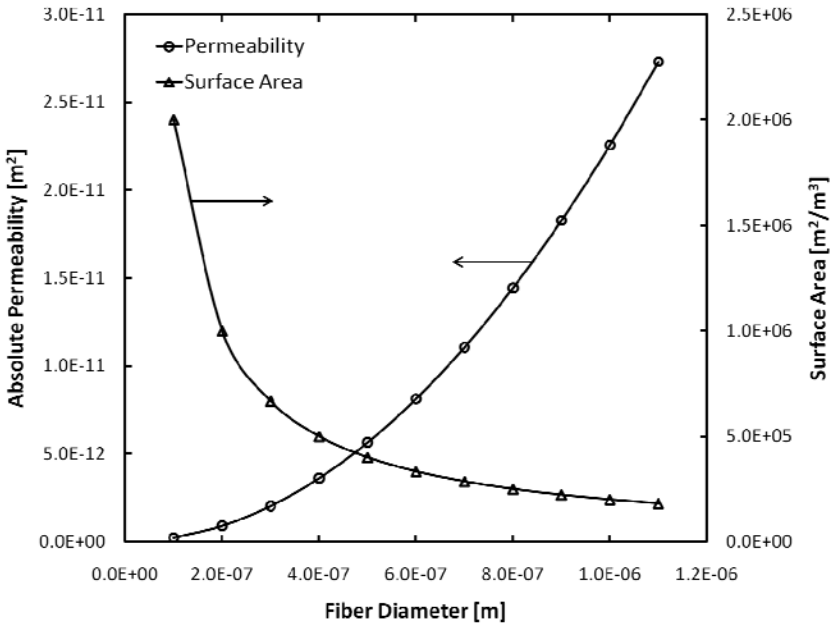

Fig. 7 Permeability and surface area of a fibrous material with a porosity of 0.8 as a function of fiber diameter. Permeability was calculated using the Carman-Kozeny model and surface area was estimated using the filament analogue model.

Another aspect of the active solid surface area that must be considered is the intimacy of the solid/electrolyte contact [18, 36]. Carbon and graphite materials have a neutral wettability to water [111] which prevents the spreading of electrolyte over the electrode surface. The trapped air pockets resulting from incomplete wetting reduce the electroactive surface area owing to the Cassie-Baxter effect. Such incomplete wetting would be exacerbated on roughened surfaces. Sun and Skyllas-Kazacos found that certain electrode pretreatments intended to improve catalytic activity also lead to somewhat improved wettability behavior [36]. Litster *et al* [112] report that briefly heating carbon fiber materials at 300 °C in an air environment rendered them fully

hydrophilic, and Yan *et al* [113] review various treatment procedures for altering carbon contact angle. The presence of a gas phase at the solid/electrolyte interface could be due to residual air trapped during initial flooding of the electrode, or could appear due to evolution of gases such as the parasitic evolution of hydrogen and/or oxygen [13, 114].

4. Transport Phenomena

There are various mechanisms of transport that occur within a RFB. Typically, electron flow is not limiting due to the use of conductive additives or just carbon materials. This transport is adequately described by Ohm's law,

$$\mathbf{i}_1 = -\sigma \nabla \Phi_1 \tag{27}$$

where σ is the electronic conductivity. The other major transport issue is that of the reactants and products. Typically, this can be separated into two different regions, namely, that of the electrode and that of the membrane or separator. These two regions often have different properties; their transport species and mechanisms are discussed in turn below. For the electrolyte in the electrodes, diffusion is often the most important process while conduction is for the membrane. Table 3 shows a summary of the charge-carrying species across the membrane, open circuit potential, and diffusivities of active ions. While dilute-solution theory does not necessarily strictly apply in the electrolyte systems of interest, diffusivities of the ions give a good indication of the relative motions of the relevant ions. Cation-exchange membranes (mainly H^+ and Na^+) are widely used in the aqueous RFBs due to their high ionic conductivity. Anion exchange membranes are used in many non-aqueous systems to be compatible with the supporting electrolytes used and suppress unwanted crossover. Generally, the open-circuit potential of an aqueous system is constrained to be lower due to the low electrochemical stability

window of H_2O compared to that of non-aqueous RFB's, in which organic solvents (such as acetone) with a higher electrochemical stability voltage window are used. The diffusivities of active species in all systems listed in Table 3 are in the range of 1.6 to 12×10^{-6} cm^2/s except for V(IV) (1770 $\times 10^{-6}$ cm^2/s in 6.4 M HBr and 2M HCl). Finally, while there are some other, less critical issues such as thermal management and heat transport within the cell, such a discussion is beyond the scope of this review.

Table 3. Summary of different thermodynamic and transport parameters for various RFBs.

RFB	Membrane charge carrier	Open-circuit potential (V)	Diffusivity, D (10^{-6} cm^2 s^{-1})		Ref.
All vanadium	H^+	1.26	$VCl_3+H_2SO_4/Na_2SO_4$, glassy carbon electrode	1.50 (pH=4.0) 1.34 (pH=2.0) 1.16 (pH=1.0) 1.41 (pH=0.0)	[29]
			V_2O_5+1.8 M H_2SO_4/Na_2SO_4, glassy carbon electrode	5.7	[29]
Vanadium/bromine	H^+	1.1	V(IV) + 6.4M HBr, 2M HCl solution	1770	[50]
Iron/chromium	Cl^-/H^+	0.77 to 1.03	Fe(III)	6	[19]
			Cr(III)	6	
Zinc/bromine	H^+	1.85	Zn^{2+}	7.54	[58]
Zinc/cerium	H^+	2.2	Ce(III) ion in methanesulfonic acid	0.27–0.72	[118]
Bromine/polysulphide	Na^+	1.54	Br^-	12	[22]
			Br_3^-	5	
			S_2^{2-}	6	
			S_4^{2-}	5	
Fe(III)/Fe(II) triethanolamine/bromine	Na^+	1.0	N/A	1.63	[64]
Non-aqueous Vanadium acetylacetonate	BF_4^-	2.2	$V(acac)_3$	1.8–2.9	[67]

4.1 Electrolyte flow

Within the electrode, the flux of the various species can be described using the Nernst-Planck equation assuming that dilute-solution theory holds [115]

$$\mathbf{N}_i = -z_i u_i F c_i \nabla \Phi_2 - D_i \nabla c_i + c_i \mathbf{v} \tag{28}$$

The first term in the expression is a migration term, representing the motion of charged species that results from a potential gradient. The migration flux is related to the potential gradient ($-\nabla\Phi_2$) by a charge number, z_i, concentration, c_i, and mobility, u_i. The second term relates the diffusive flux to the concentration gradient. The final term is a convective term and represents the motion of the species as the bulk motion of the solvent carries it along. For noncharged reactants and products (e.g., Br_2), the same equation can be used with the migration term set to zero, resulting in the equation of convective diffusion [116]. Dilute-solution theory considers only the interactions between each dissolved species and the solvent, and thus one can consider the conductivity of the solution to be given by

$$\kappa = F^2 \sum_i z_i^2 c_i u_i \tag{29}$$

The motion of each charged species is described by its transport properties, namely, the mobility and the diffusion coefficient. These transport properties can be related to one another at infinite dilution via the Nernst-Einstein equation [115, 117, 118]

$$D_i = RTu_i \tag{30}$$

For more complicated systems than binary electrolytes or where the interactions between species are important and/or non-ideal, concentrated-solution theory can be used as discussed by Newman and Thomas-Alyea [115]. In this approach, the transport coefficients of merit include the conductivity of the solution, and the transference numbers and diffusivities of the ions. It

should be noted that many RFBs operate at higher concentrations such that concentrated-solution theory may be required; however, the use of supporting electrolytes does mitigate this to a certain extent in that detailed speciation is not required to predict cell performance fairly well.

The total current in the electrolyte can be expressed as

$$\mathbf{i}_2 = F\sum_i z_i \mathbf{N}_i \tag{31}$$

and the ionic conductivity of the electrolyte can be related to the above transport properties [115].

For most RFB applications, the system is one phase (liquid) and so complicated expressions for multiphase flow are unnecessary, in stark contrast to low-temperature fuel cells [119]. Thus, for the convective flow one can use the Navier-Stokes equations [116]

$$\mathbf{v}\cdot\nabla(\rho\mathbf{v}) = -\nabla p + \mu\nabla^2\mathbf{v} \tag{32}$$

where p is the pressure, and μ and ρ are the viscosity and density of the liquid, respectively. Since most RFB electrodes are porous, the above equation can be extended using various methodologies such as Brinkman [109, 116, 120], or even replaced by Darcy's law [109]

$$\mathbf{v} = -\frac{k}{\mu}\nabla p \tag{33}$$

Flowing electrolyte through porous electrodes presents a number of challenges, both at the single cell and full stack level. At the pore scale within each electrode there will be significant differences in the interstitial flowrate in each pore owing to size differences, with flow largely confined to the largest pores in the medium. Such pore-scale-channeling behavior provides convective mass transport at a limited number of surfaces, while dead zones of relatively stagnant flow and localized limiting currents would exist elsewhere throughout the electrode.

Fibrous materials are the favored porous-electrode substrate for several reasons because high porosity can be achieved while still maintaining electrical conductivity and percolation in the solid phase due the bridging between long fibers. As discussed above, high porosity is advantageous since (a) there is a strong positive correlation between porosity and permeability [114], thereby resulting in reduced pressure drop and associated pumping costs; and (b) the effective ionic conductivity of the electrolyte is directly proportional to porosity [121] and inversely proportional to tortuosity which tends to increase with decreasing porosity [114].

Due to the wide spread use of fibrous electrodes for various applications, a number of studies have looked at mass transfer in carbon-fiber electrodes [67, 122, 123, 124 , 125]. Schmal *et al* [67] compared mass transfer at single fibers to fiber assemblies (bundles and felts) and found that per unit length of fiber the mass transfer to a single fiber was significantly higher. This was attributed to channeling within the fiber assemblies causing dead-zones or stagnant regions, effectively reducing the active area for reaction. A porous material with very uniform pore-size distribution would help alleviate this problem, but such materials may be impractical. Saleh [126] studied the effectiveness factor in packed bed electrodes and found that ohmic resistance, which is a combination of fluid properties and bed geometry, also played a key role in determining the extent to which the porous electrode was utilized.

Another cell-scale issue arising from the convective flow in porous electrodes is large scale heterogeneities due to assembly tolerances or uneven thermal expansion, which could lead to bypassing of large sections of a cell. Moreover, flow through porous electrodes presents major manifolding issues at the stack-scale since each cell must have nearly identical permeability. This would be difficult to achieve since stacks may be compressed significantly when assembled. This situation is analogous to interdigitated flow fields proposed for low-temperature fuel cells,

which showed very promising performance results in single-cell tests, but the inevitable differences in permeability from cell to cell in a stack created uneven flow distribution among cells [127].

To enhance flow and electrolyte utilization during deep discharge where high flow rates are required, physical barriers or roughened electrode materials can be used inside the cell to promote turbulence and mass transport. Lessner *et al*. designed a flow-through porous electrode for bromine/polysulphide RFBs [24]. To ensure uniform flow distribution and prevent channeling, quartz particles (with diameter of 0.5–1.0 mm) were placed 0.5 cm above the inlet. Based on the results, the relationship between dimensionless mass transfer rate (Sherwood number, Sh) and Reynold number (Re) for their geometry was obtained

$$\mathrm{Sh} = 14.29\,\mathrm{Re}^{0.348} \tag{34}$$

This functional dependence on Re is in excellent agreement with Sioda's [128] and Cano and Bohm's [129] findings.

Leung *et al.* also investigated the effect of the mean linear flow velocity of the electrolyte on the cell performance both under constant current charge and discharge [71]. Fig. 8 presents the effect of the mean linear flow velocity on the discharge voltage with different constant discharge current densities. It is shown that there is a maximum cell voltage at the mean linear flow velocity of 3.9 cm s^{-1}.

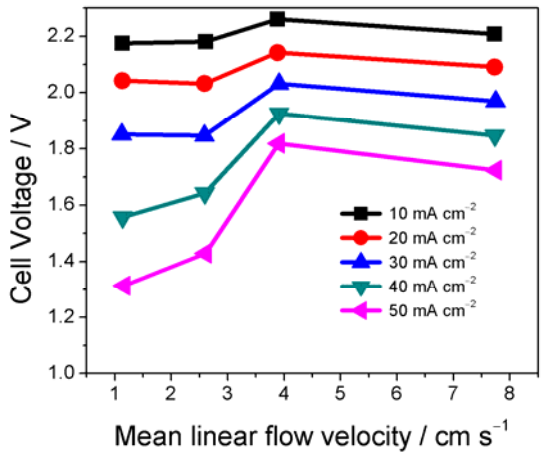

Fig. 8. Effect of the mean linear flow velocity of the electrolyte on the cell voltage of the Zn/Ce RFB. Adapted from reference [71] with permission.

4.1.1 Reactant concentration effects

The issue of reactant solubility in the flowing electrolyte solution can be important. The energy density of a RFB system is set by the concentration of dissolved species, but the maximum concentration in any stream is limited by the solubility of the least soluble species. Precipitation of reactants or products in the porous electrode is calamitous. Concentration limits on the electroactive species not only reduces the energy density of a system, but also negatively impacts the power density and cell efficiency as well. Lower concentrations mean reduced mass-transfer rates and current density, thus increasing concentration polarization and/or pumping power. Solubility is a function of temperature as well, which must be factored into cell design. For instance, it is observed that V_2O_5 precipitation occurs at elevated temperature, limiting the operating temperature to the range of 10 to 40 °C [37, 130]. Li *et al*. improved this situation with the development of a vanadium sulfate and chloride mixed electrolyte, enabling a vanadium concentration up to 2.5 M over a temperature range of –5 to 50°C [46]. However, temperature excursions in an operating cell could cause a precipitation event and lead to cell failure [18].

Other issues regarding concentrations include the fact that for many systems increasing the concentration of the reactants can lead to more complexing and lower diffusivities and perhaps even more viscous solutions. For example, recent data measured at LBNL show that Br_2 diffusivity decreases by a factor of two as the concentration of HBr is increased from 1 to 7 M [131]. Such tradeoffs require optimization for the specific system. Another ubiquitous issue present in flowing reactors of all types concerns the extent of reactant conversion, sometimes referred to as utilization or stoichiometry. The difficulty is determining the optimum reactant concentration at the outlet of the electrode. It is desirable or necessary that the electrode near the outlet is not starved of reactant to prevent parasitic reactions such as gas evolution or electrode corrosion. On the other hand, fully consuming or utilizing the reactants means recovery of the maximum amount of energy stored in the solution. For many systems, the stoichiometry is high for single-cell studies (typically over 10) [59], and it is not clear as to how this can be translated into actual systems where such performance would necessitate multiple passes through the electrodes. One such approach would be to have a cascade of reactors that are tailored to specific operating points and concentrations [132].

4.1.2 Shunt currents

One of the challenges of stack design that must be given particular attention in redox flow battery configurations is protection against shunt currents. Generally speaking, a shunt current refers to a condition in which current deviates from the intended path, via a parallel path with a sufficiently low resistance to divert a portion of the current. In general, the path of least resistance in a cell or stack is designed to follow the direction of intended current flow. In a flow battery configuration in which cells are configured in series, it is intended for all of the current to flow in the electrolytic phase via ionic conduction from one negative electrode to the

adjacent positive electrode, and in the current collector from one adjacent bipolar plate to another. In a well-designed stack, there should be no current flow except directly from one cell to another in the preferred series configuration.

In practice, however, there is no perfectly insulator, and current can flow from one cell to another in such a way that significant power is lost and stack output voltage is lowered. It is possible for stray electronic paths to allow redistribution of current from one cell of a multicell stack to another, and strict requirements on the resistance of stack externals such as manifolds and packaging help to minimize shunt currents via electrical conduction [133]. The same general rules and restrictions that guide conventional battery and stack design and isolation can prevent shunt currents via electrically conducting pathways.

Of particular concern in flow batteries is the development of shunt currents via the liquid electrolyte. While shunt currents can develop in the liquid phase in conventional fuel cells and battery designs [134, 135], the restriction of the primary electrolyte to the region between each pair of current collectors minimizes most obvious paths for current flow, at least in the electrolytic phase. While fuel cells do distribute fluids from one cell to another via the fuel manifolds, the effective conductivities of liquid-feed fuels and of most coolants are much lower than the conductivities of flow battery electrolytes [18, 136].

Because RFBs involve the circulation of electrolyte to each of the individual cells, there is an obvious ionic current path from one cell to another. The currents that flow in the circulating electrolyte from one cell to another via the electrolyte flow manifolds are best managed by increasing the effective resistance of the flow path, either by increasing the effective path length between cell flow inputs and outputs in the manifold, or by reducing the cross- sectional area of the ports. Unfortunately, increasing the resistance in such a way to minimize shunt currents also

works to increase the resistance to flow. This has the result of increasing the requirements for parasitic power to circulate the electrolyte through the system; this complicates system design and increases both capital and operating costs. Several researchers have investigated the design implications for flow batteries for particular systems, though optimization will be required for specific electrolyte and cell configurations [137-139].

4.2 Separators

There are two main types of RFB separators. The first is a microporous separator that can allow for exchange of liquids between the anolyte and catholyte compartments. Such an approach is akin to the discussion above concerning a porous region. Because of this ability to mix, microporous separators often lead to higher rates of reactant and product crossover, and thus lower coulombic efficiencies. For this and other reasons, most RFBs use an ionically conducting membrane as a separator.

The ion-exchange membrane (IEM) is one of the most critical components in RFBs. In terms of transport, the dual and opposing needs to enhance the desired charge transport while limiting undesired crossover of reactant, product, and other species is an unresolved engineering issue. There are a number of IEMs which have been used in RFBs, with the most common one being Nafion®, a perfluorosulfonic acid membrane that binds cations to its sulfonic acid sites [140]. Nafion® is the membrane of choice in many RFBs due to its high proton and sodium conductivities and its proven stability in the chlor-alkali industry. It has a conduction mechanism that includes both hopping and vehicular modalities.

Since most IEMs are single ion conductors (see Table 3), transport within them can often be described using Ohm's law (equation 27). If there are other interactions such as

electroosmotic flow, this description can be modified; for example, for proton conduction in Nafion® the following expression can be used [141, 142]

$$\mathbf{i}_2 = -\kappa \nabla \Phi_2 - \frac{\kappa \xi}{F} \nabla \mu_0 \tag{35}$$

$$\mathbf{N}_0 = -\frac{\kappa \xi}{F} \nabla \Phi_2 - \left(\alpha + \frac{\kappa \xi^2}{F^2} \right) \nabla \mu_0 \tag{36}$$

where ξ is the electroosmotic coefficient, κ is the ionic conductivity, μ_0 is the chemical potential of the solvent, and α is the transport coefficient of the solvent through the membrane. If there are other ions in the solution that penetrate the membrane, it is easiest to describe this motion using a Poisson-Nernst-Planck (PNP) framework where the Nernst-Planck equations are used (equation 28) along with Poisson's equation,

$$\nabla^2 \Phi_2 = -\frac{\rho}{\varepsilon_0} \tag{37}$$

where ε_0 is the permittivity and ρ is the charge density. This methodology accounts for non electroneutrality conditions that exist due to the small charged pathways inside the membrane for conduction. In the above PNP treatment, dilute-solution theory is used and if interactions between species and non-dilute behavior is expected, one can use concentrated-solution theory, which complicates the expressions, requires more knowledge of the transport properties, and is beyond the scope of this paper (for an example, see Delacourt and coworkers [143, 144]). In terms of reactant and product crossover, the easiest way is to use a permeation coefficient, ψ, which is a combination of Henry's law and a transport coefficient such as a permeability,

$$\mathbf{N}_i = \psi_i \nabla c_i \tag{38}$$

Membrane design should consider the following properties: ion conductivity, ion selectivity,

permeability, chemical stability, and mechanical properties. A detailed summary of the recent progress of IEM for VRBs can be found in the review by Li *et al* [6] and we use the VRB as the example for discussing IEMs and transport; Table 4 shows some IEMs used for the VRB example case.

Table 4. Summary and comparison of ion-exchange membranes used in all-vanadium RFB (VRB).

Membrane	Approach	Thickness (μm)	IEC* (mmol/g)	Permeability (ppm)			Ionic conductivity (mS/cm)	Liquid uptake (wt%)	Ref.
				V^{3+}	VO^{2+}	VO_2^+			
Nafion®/SiO_2	Hybrid	204	0.96	< 134	< 82	< 17.8	56.2	21.5	[145]
Modified Nafion®117	Interfacial polymerization	201	0.88	-	34.6	-	15	-	[146]
SPEEK	Blend	88	1.76	-	12.4	-	7.5	28.6	[147]
PVDF-g-PSSA-co-PMAc	Radiation grafting	70	1.95	11.2	0.73	1.1	100	22	[148]
AIEM	Two-step radiation-induced grafting	42	0.97	-	22	-	31	25.4	[149]
SPFEK	Non-fluorinated	-	1.92	-	< 125	-	34.8	20.5	[150]
SFPEK	Non-fluorinated	151	1.59	-	94	-	2.2	36	[151]
SPTK	Non-fluorinated	-	1.29	-	12	-	10.5	11.9	[152]
SPTKK	Non-fluorinated	-	1.91	-	31	-	13.6	19.3	[152]
Nafion®117	PFSA	178	0.94	< 600	< 550	< 120	58.7	26.0	[153]
Nafion®115	PFSA	127	0.91	-	79.5	-	13.4	26	[147]

* IEC: ion exchange capacity

Skyllas-Kazacos *et al*. used the Amberlite CG 400 composite membrane in the VRBs. The membranes showed a good stability with more than 4000 hours [43, 44]. Zhang *et al*. found that the current efficiency of 94 and 91 % are achieved for Nafion® 115 and 112 membranes used in VRBs, respectively [5]. However, the Nafion® membranes suffer from heavy active ion crossover and low ion selectivity. By incorporation of inorganic species (such as SiO_2, TiO_2, and ZrP) into Nafion®, the crossover of vanadium ions can be effectively reduced [145, 146, 154]. The ion selectivity can be enhanced using the organic/ Nafion® hybrid membranes fabricated

with interfacial polymerization and directly blending methods. Xi *et al*. prepared Nafion®/SiO_2 hybrid membranes using *in situ* sol-gel method, and showed that the vanadium crossover was effectively reduced due to the polar clusters of the original Nafion® [146]. The maximum energy efficiency of the VRB using this membrane was nearly 80% at 20 mA/cm^2. Luo *et al*. modified Nafion®117 membrane using interfacial polymerization method for VRB application [155]. Sulfonated poly(tetramethydiphenyl ether ether ketone) (SPEEK) membrane showed one order of magnitude of vanadium ion permeability lower than that of Nafion® 115 [147]. In the multiple-cycle tests, the SPEEK40 membrane shows high stability and high columbic efficiency above 98%. Generally, IEMs prepared with interfacial grafting, blend, radiation, non-fluorinated and hybrid membranes show lower ion permeability than that of Nafion® membrane. However, when V^{n+} crossover is blocked, the protonic conductivity is also decreased which results in relatively low conductivity. So it is still a critical challenge for IEM development that ion selectivity is enhanced with high ionic conductivity. Vafiadis and Skyllas-Kazacos assessed a range of IEMs in vanadium/bromine RFBs considering ion-exchange capacity, conductivity, vanadium ion diffusion, water content, and chemical stability [51].

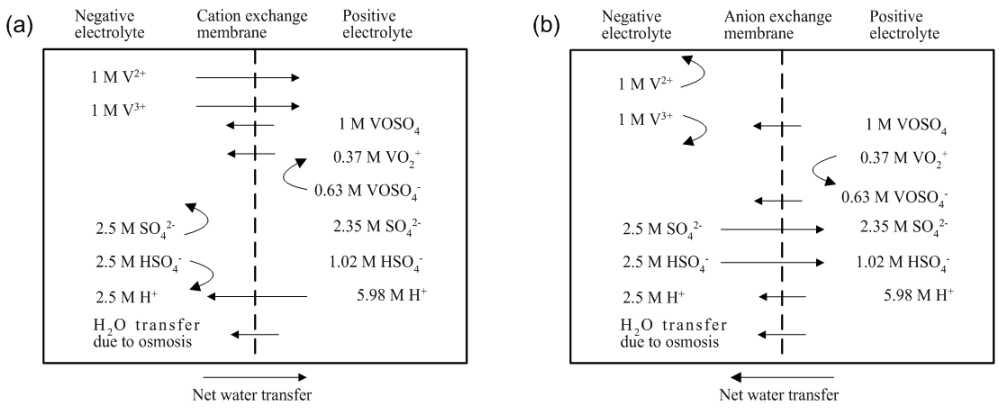

Fig. 9. Various fluxes across cation exchange membrane (a) and anion exchange membrane (b) for the vanadium electrolyte solutions [44].

In addition to ion transfer, electroosmotic flow can cause transfer of water from one half cell to the other one during the charge-discharge cycles. The direction and magnitude of the transport is affected by the membrane used. Mohammadi *et al*. studied the water transfer behavior of anion- and cation-exchange membranes in the VRB [43]. As shown in Fig. 9, a significant amount of water is transferred from the negative-half-cell electrolyte to the positive half cell in a VRB using a cation-exchange membrane such as Nafion®. This movement is attributed to the hydration shells of V^{2+} and V^{3+} ions which carry a large amount of water and can easily permeate through cation-exchange membranes. For anion-exchange membranes, the permeation of V^{2+} and V^{3+} co-ions are restricted. However, there is a net water transfer from the positive half cell to the negative half cell because of the neutral $VOSO_4$ and negative $VO_2SO_4^-$ in the positive half cell that can readily permeate through the membrane [44].

5. Cell modeling and design

The above two section describe transport and kinetics. These descriptions can be combined in overall mass conservation equations of the individual species to track where and how they move through the system [119]

$$\frac{\partial(1-\varepsilon)c_i}{\partial t} = -\nabla\cdot\mathbf{N}_i - \sum_h a_{1,2}s_{i,k,h}\frac{i_{h,1-2}}{n_hF} + \sum_l s_{i,2,l}\sum_{p\neq 1} a_{2,p}r_{l,p} + \sum_g s_{i,2,g}(1-\varepsilon)R_g \qquad (39)$$

The term on the left side of the equation is the accumulation term, which accounts for the change in the total amount of species *i* held in phase *k* within a differential control volume. The first term on the right side of the equation keeps track of the material that enters or leaves the control volume by mass transport. The remaining three terms account for material that is gained or lost due to chemical reactions. The first summation includes all electron-transfer reactions that occur at the interface between phase *k* and the electronically conducting phase (denoted as phase 1).

The second summation accounts for all other interfacial reactions that do not include electron transfer, and the final term accounts for homogeneous reactions in phase *k*. In the above expression, ε is the porosity of the domain, $s_{i,k,l}$ is the stoichiometric coefficient of species *i* in phase *k* participating in heterogeneous reaction *l*, $r_{l,p}$ is the rate of the heterogeneous reaction *l* per unit of interfacial area with phase *p*. R_g is the rate of a strictly homogenous reaction *g* per unit volume.

The key component in a RFB is the porous electrode where the reactions occur. The fundamentals behind porous electrodes are well established by the work of Newman and coworkers [115, 156]. A porous electrode can be visualized as a resistor network as shown in Fig 10.

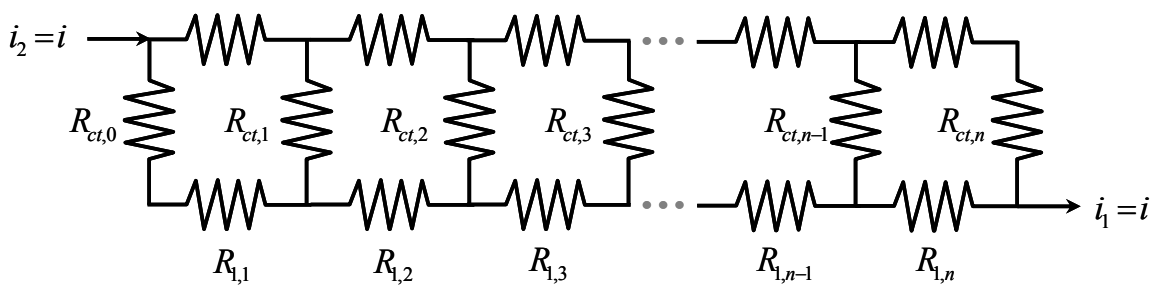

Fig. 10. Steady-state resistor-network representation of porous-electrode theory.

In Fig 10, the total current density, *i*, flows through the electrolyte phase (2) and the solid phase (1) at each respective end. In between, the current is apportioned based on the resistances in each phase and the charge-transfer resistances. The charge-transfer resistances can be nonlinear because they are based on kinetic expressions. Thus, the reaction will proceed depending on what is limiting. Since kinetics are typically facile in RFB systems, the main issues are reactant and ion movement to and away from the reaction site. For example, if the mass-transfer of a reactant is limiting, then the reaction will proceed near the inlet, whereas if ion conduction is

limiting, then it will occur near the separator; a uniform reaction rate is rarely achieved without some kind of mass-transfer control (e.g., a microporous layer limiting flow of a reactant). An interesting issue is that one cannot diagnose what is limiting purely from a polarization curve, since even mass-transfer limitations can appear to be ohmic ones. For example, due to reactant mass-transfer limitations, a reaction may proceed at the electrode surface near the flow inlet yet the performance will look as if it is ohmically limited due to the distance the ions have to travel from the separator to the reaction site. Because of this and other reasons, mathematical modeling is often used to understand the limiting phenomena and processes in a RFB; yet, relative to the experimental and demonstration system development, analytical and computational modeling of RFBs has trailed, which may be due to the era in which they were heavily researched. Advanced modeling is needed to understand fully the various physiochemical phenomena involved to help minimize transport losses and facilitate optimized material design and architectures. The models help lead to optimized porous-electrode structures, which are crucial in increasing RFB performance and hence reducing cost. These issues are explored in more detail in this section.

5.1 Electrode structure

RFB can have two basic electrode configurations: flow through a porous 3D electrode or flow past a planar electrode. These are shown schematically in Fig 11(a) and (b) respectively. Naturally, these two configurations are often referred to as 'flow-through' and 'flow-by' electrodes, but this terminology is somewhat confusing since these two terms are also occasionally used to describe flow parallel and perpendicular to the direction of the current flow [157]. The following discussion will adopt the intuitive use of 'flow-through' a porous electrode and 'flow-by' a planar electrode.

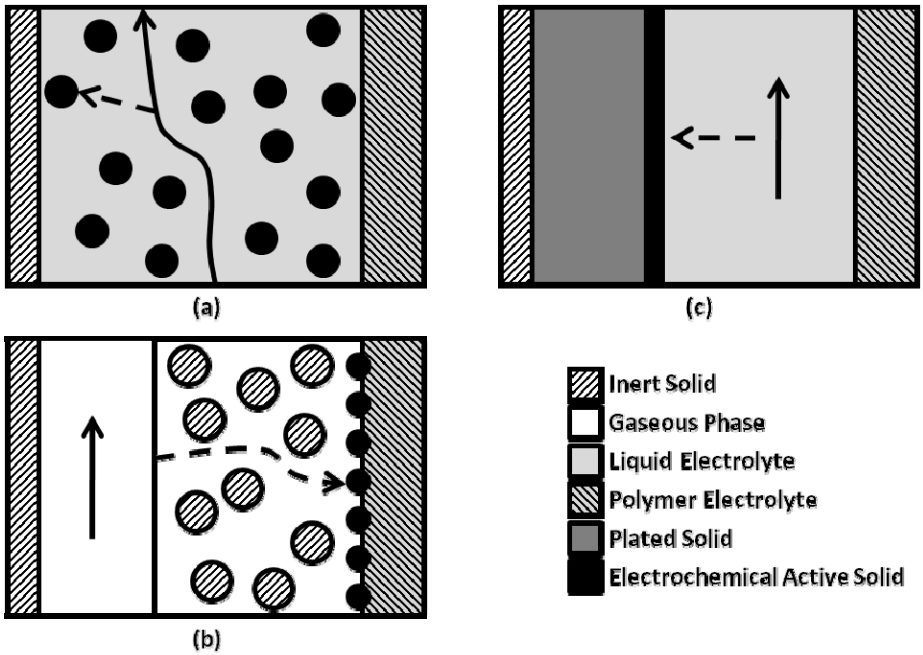

Fig. 11. Schematic diagrams of (a) flow through electrode, (b) flow-by electrode with active surface near the current collector (left) and near the membrane separator (right), and (c) flow-by electrode used in solid-plating cells. Solid arrows indicate convective flow of reactants and dashed arrows represent diffusive paths.

Whether a flow-through or a flow-by electrode can or must be used depends on a number of factors including the physical state of the flowing reactant (i.e. gas or liquid), the electrode reaction occurring (e.g. plating of solid or electron transfer in solution) and the conductivity of the electrolyte phase. For instance, in the prototypical or conventional RFB [57, 58] the reactants and products on both the anode and cathode are dissolved ions, and a porous 3D flow-through electrode, as shown in Fig 11(a), is typically used on both sides. In this configuration the liquid electrolyte flows through a porous matrix of electrochemically active solids, usually carbon fibers with appropriate catalytic surface properties. The ions produced by the reaction migrate through the electrolyte phase toward the opposing electrode and the electrons move through the network of carbon fibers to the current collector. The flow-through electrode is well suited to reactions of flowing liquid-phase species for a number of reasons. First, the diffusivity of liquid-phase species is quite low so forced convection through a porous electrode provides enhanced

mass-transfer rates. Second, the concentration of reactive ions is generally low due to solubility limits so forced mass transfer helps maintain higher current densities. Finally, the flowing electrolyte will generally have a high ionic conductivity, which is necessary to avoid ohmic polarization losses over the long transport lengths created by the 3D configuration.

The planar electrode is most commonly used when a gaseous reactant is involved. A common example is the hydrogen/bromine cell [72] which uses a liquid mixture of bromine and aqueous hydrobromic acid on the cathode with a flow-through electrode (Fig 11(a)) and gaseous hydrogen on the anode, with a flow-by electrode as shown in Fig 11(b). In this configuration a gaseous species flows in a channel parallel to the electrode and diffuses laterally to the essentially planar electrode surface. (In reality the electrode surface is a 3D porous zone of catalyst particles and immobilized electrolyte phase, but it behaves essentially as a planar surface on the scale of the electrode assembly). The porous region of inert solid between the flow channel and the reactive surface acts to distribute gas uniformly to the catalyst and conduct electrons from the electrode to the current collector. The flow-by electrode is well suited to gaseous reactants for two reasons. First, the gaseous reactant stream does not conduct protons, so the reaction must happen at or near the electrolyte phase. Second, the diffusivity of gaseous species are 3 to 4 orders of magnitude higher than liquid-phase species so diffusive mass transfer is able to supply reactants to the electrode at a sufficient rate. Another variant of the flow-by electrode is shown in Fig 11(c), which is used when a solid is electrochemically plated out or dissolved as in the hybrid RFBs. Because the electrode grows during plating, it is not feasible to use a porous electrode as it would become plugged by the plating solid. The so-called single-flow cell reported by Pletcher, Wills and co-workers [2, 72] uses a solid electrode on both the anode and cathode where Pb and PbO are stored as plated solids. Ion conduction through the

flowing electrolyte phase to the opposing electrode is at a maximum distance in this configuration so ohmic losses are high. Also, the surface area for reaction is at a minimum and equal to the geometric area of the cell. Consequently, this type of flow-by electrode is only used when absolutely necessary, as is the case of the aforementioned solid-plating electrodes.

The use of planar flow-by electrodes with liquid-phase reactants to demonstrate the viability of RFB technology is not uncommon in research papers on the subject [25, 63, 102], but flow-by electrodes, due to their limited surface area and long ion-transport distances, would almost never be preferred over 3D electrodes occupying the same volume. Even in the original RFB patent by Thaller [42], the possibility of using porous, 3D electrodes was included. Many of the tradeoffs of the various geometric placements and concerns can be found in the literature, including the pioneering work of Trainham and Newman [158-160] who examined optimum electrode placement and the tradeoffs between the two transport resistances in Fig 10.

5.2 Cell modeling of certain chemistries

5.2.1 Iron/chrome

Fedkiw and Watts developed a mathematical isothermal model to describe the operation of a single anode-separator-cathode Fe/Cr cell based on electrode theory, redox kinetics, mass transfer, and ohmic effects. The parasitic hydrogen reaction was also considered [161]. It is found that the separator ohmic resistance is the dominant cell resistance followed by the electrolyte ohmic resistance. The kinetic resistance was determined to be negligible at reasonable flow rates. It was predicted that countercurrent electrolyte flow improves global cell performance due to a more uniform current distribution. Decreasing the electrode area tended to decrease the cell current but resulted in high velocity and enhanced mass transfer within the penetration thickness and increased current. This model also provided a method of determined a charge-

discharge protocol that obtained the maximum chromium conversion and minimum hydrogen evolution at the same time [161, 162]. Finally, Codina *et al* [137] examined the issue of shunt currents when a cell is scaled up to larger sizes and stacks.

5.2.2 All vanadium (VRB)

Not surprisingly, the VRB is the most often modeled RFB, especially recently [163-169]. Shah *et al*. developed a two-dimensional transient model validated against the experimental diurnal data to study the effects of variation on concentration, electrolyte flowrate, and electrode porosity [170]. They also studied the effects of H_2 and O_2 evolution on the performance of VRBs by dynamic modeling [166, 167, 171]. As shown in Fig. 12, numerical simulation demonstrates good agreement with the experimental data [171].

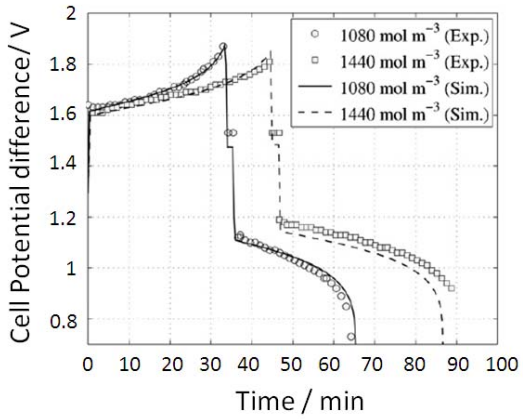

Fig. 12. A comparison between simulated and experimentally obtained cell potential difference. Adapted from Ref. [171] with permission.

Evolved H_2 and O_2 in the form of bubbles on the negative and positive electrodes, respectively, impact performance through partial occlusion of the electrolyte flow, reduction in the active surface area for reaction, and reduced mass- and charge-transport coefficients. You *et al*. built a two-dimensional stationary model to describe a single VRB flow cell [169]. They found the decrease in the mass transfer coefficient almost has no effect on the distribution of V^{3+} concentration and overpotential, as shown in Fig. 13. Li and Hikihara developed a model

considering the transient behavior in a VRB and the model was also examined based on the tests of a micro-RFB [172]. They found that the chemical reaction rate is restricted by the attached external electric circuit and the concentration change of vanadium ions depends on the chemical reactions and the flow of electrolysis solution.

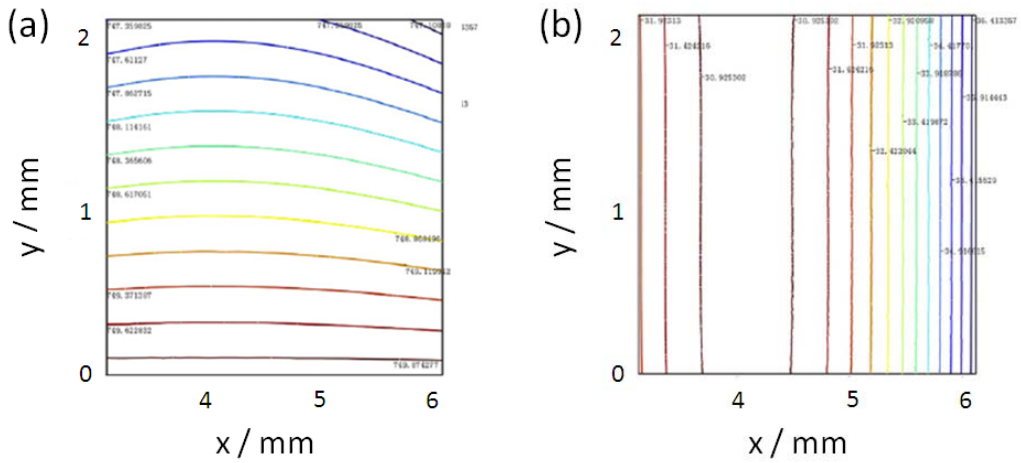

Fig. 13. Profiles of V^{3+} concentration (a), and over-potential (b) inside in the negative electrode at 50% SOC with the applied current density of 40 mA/cm^2. Adapted from ref [169] with permission.

5.2.3 Bromine/polysuphide

Scamman *et al*. developed a numerical model that can be used for the design and optimization of large-scale bromine/polysulphide RFBs [173, 174]. They used the Butler-Volmer equation to estimate overpotential losses. The crossover of active species and self-discharge was also considered. This model is able to predict the concentration and current variation along the electrode and determine various efficiencies, energy density, and power density in the charge-discharge processes. It is found that the electrochemical rate constants of the bromide and sulphide are 4×10^{-5} and 3×10^{-6} cm/s, respectively.

5.2.4 Zinc/bromine

Several models of Zn/Br_2 have been developed to understand the physical phenomena and to determine how cell performance can be improved. These models have been used to investigate

the species transport, secondary electrode reactions, and chemical reactions in the bulk electrolyte, including issues during the plating of zinc [175]. Putt [176] and Lee and Selman [177] developed thin diffusion-layer models. These models include electrolyte convection with Butler-Volmer kinetics. Mader and White [61] developed a mathematical model for the cell mainly to predict performance of the cell as a function of architecture and operating conditions. They also used their model to determine the effects of the mass transfer and electrokinetics in the porous bromine electrode on the roundtrip performance of the cell. It was found that the cell efficiency increases with the porous electrode thickness. Jorne and coworkers [178, 179] also developed models for the chlorine electrode in a Zn/Cl_2 cell. This electrode is very similar to the bromine one and they showed that the flow from the gap to the zinc electrode can impact the current density and reaction-rate distribution significantly, as well as the placement of the electrode as shown in Fig. 14.

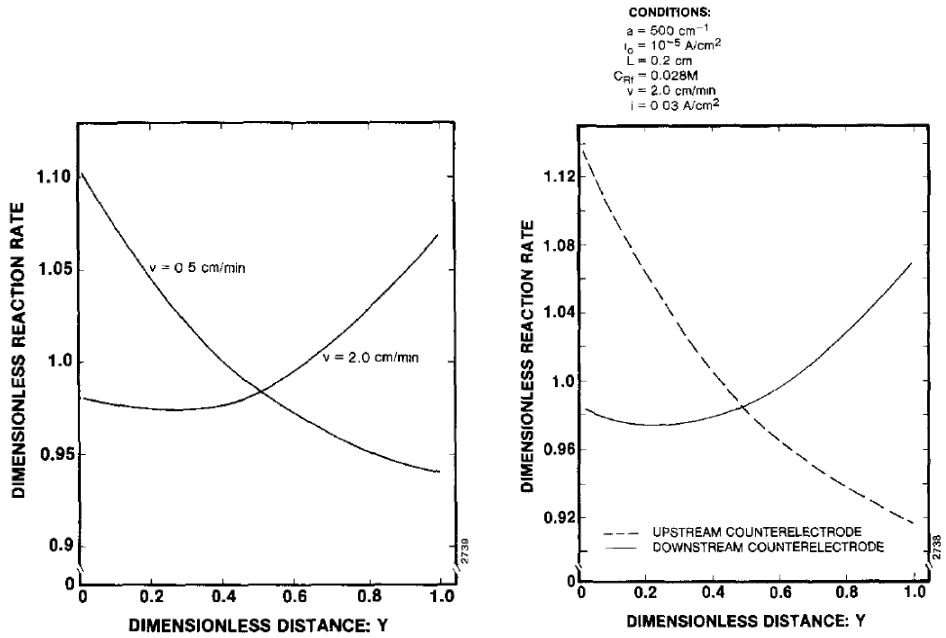

Fig. 14. Reaction-rate profiles for a Cl_2 discharging elect rode in a Zn/Cl_2 RFB at (a) different flow velocities and (b) electrode placement. Adapted from ref [179] with permission.

5.2.5 Zinc/cerium

Trinidad *et al*. developed an oxidation-reduction-redox-potential model to monitor the Ce(III)/Ce(IV) couple [180]

$$E_e = E_e^0 - \frac{RT}{zF}\left\{kt + \ln\left[\frac{(C_{Red})_0}{(C_{Oxd})_0} + (1 - \exp(-kt))\right]\right\} \quad (40)$$

The redox potential *vs*. time experimental and model predictions were compared as shown in Fig 15. The model fit well with the experimental results, showing the model is useful to predict concentration versus time in a simple redox system.

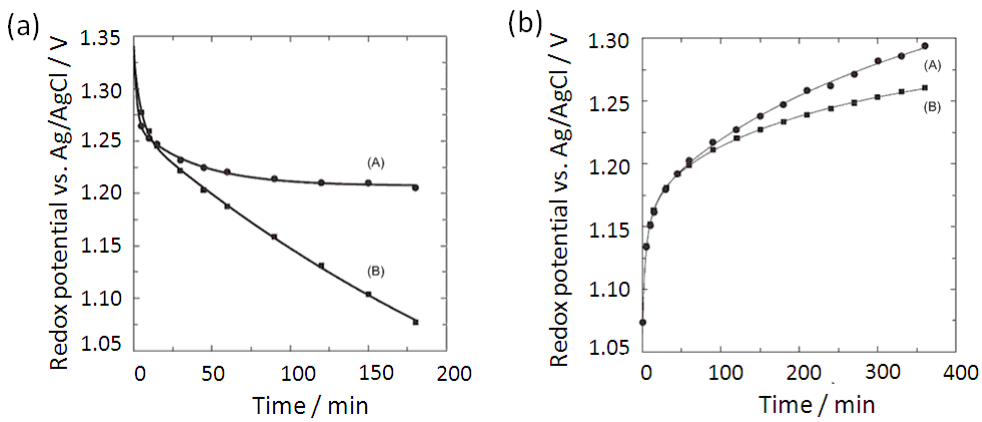

Fig. 15. (a) Redox potential *vs*. time for the reduction of 0.043 M of Ce(IV) in 1 M H_2SO_4 for both experimental (A) and calculated (B) values. (b) Redox potential vs. time for the reduction of 0.127 M Ce(III) in 1 M H_2SO_4 and 0.046 M of Ce(IV). Adapted from ref [180] with permission.

6. Summary and future research needs

In this review, we have examined some of the more common redox flow batteries (RFBs) and their individual components and underlying governing physical phenomena. At the present time, there is no "best" RFB chemistry; development continues through industrial and academic research supported by government and industry. It is clear that industrial development of prototypes and working systems has outpaced the fundamental research at this point. Inevitably, for the science to progress and the underlying fundamental problems to be resolved, much more

fundamental understanding is required. In terms of transport from a generic, chemistry-agnostic perspective, much more in-depth and fundamental study and characterization of the following are needed through combined experimental and analytical or computational modeling:

- Charge transport and electrochemical reaction at and near the electrode surface.
- The complex charge transport and nonidealities in the various electrolytes used.
- Species charge transport and crossover in ionic-exchange membranes. For many systems, the membranes represent a key limiting component in system feasibility. Low-cost, low-permeability membranes with good ion selectivity, stability, high conductivity, and suitable mechanical properties are required.
- The fluid mechanics and transport of electrolyte through the various electrode and cell architectures including coupled reaction rates and flow distribution to determine optimal electrode structures and properties.
- Impact of fundamental speciation and nonidealitiues of the various RFB couples and electrolyte solutions.

To enable more complete studies in these areas, a new class of RFB diagnostics will also be needed. Another topic requiring future study as the systems with the greatest potential become defined is performance degradation. As in other, more studied, electrochemical-power-conversion systems, many modes of material degradation will likely be associated with transport processes that can be better optimized to promote longevity.

Finally, throughout this review not much mention has been made concerning other components within the RFB system. In particular, the typical solvents and chemistries are inherently highly corrosive due to their high ionic and perhaps protonic concentrations. Their

nature makes sealing and material selection for pumps, flowfields, pipes, etc. very difficult and expensive; finding solutions to these issues is necessary for RFB systems to gain entrance to the market.

Acknowledgements

This work was partially funded by the Assistant Secretary for Energy Efficiency and Renewable Energy, Office of Fuel Cell Technologies, of the U. S. Department of Energy under contract number DE-AC02-05CH11231; work at UTK was carried out under NSF Early Career Development Award #0644811.

Nomenclature

$a_{k,p}$ = interfacial surface area between phases k and p per unit volume, 1/cm

c_i = concentration of species, mol/cm^3

d_f = fiber diameter, cm

D_i = Fickian diffusion coefficient of species *i* in a mixture, cm^2/s

E^0 = standard cell potential, V

E_{eq} = equilibrium cell potential, V

F = Faraday's constant, 96487 C/equiv

i = superficial current density, A/cm^2

i_0 = exchange current density, A/cm^2

$i_{h,k-p}$ = transfer current density of reaction h per interfacial area between phases *k* and *p,* A/cm^2

k = permeability, m^2

k^0 = standard rate constant, varies

m = valence state

n = valence state or number of electrons transferred in a reaction

$\mathbf{N}_i$ = superficial flux density of species *i*, mol/cm^{2}s

p = pressure, Pa

$r_{l,k-p}$ = rate of reaction *l* per unit of interfacial area between phases *k* and *p*, mol/cm^{2}s

R = ideal-gas constant, 8.3143 J/mol-K

$R_{g,k}$ = rate of homogenous reaction *g* in phase *k,* mol/cm^{3}s

$R_{i,j}$ = resistance of resistor *i,j* in Figure 10 where *ct* stands for charge-transfer, Ω cm^2

$s_{i,k,l}$ = stoichiometric coefficient of species *i* in phase *k* participating in reaction *l*

t = time, s

T = absolute temperature, K

u_i = mobility of species *i*, cm^{2}mol/J-s

v = superficial velocity, cm/s

x = stoichiometric coefficient

y = stoichiometric coefficient

z_i = valence or charge number of species *i*

Greek

α = transfer coefficient

α_i = transport coefficient of species *i*, mol^2/J-cm-s

ε = porosity

ε_0 = permittivity, F/cm

ξ = electroosmotic coefficient

ρ = density, g/cm^3

ρ_c = charge density, C/cm^3

σ = conductivity of the electronically conducting phase, S/cm

η = overpotential, V

κ = conductivity of the ionically conducting phase, S/cm

μ = viscosity, Pa-s

μ_i = (electro)chemical potential of species *i*, J/mol

Φ_k = potential in phase *k*, V

ψ_i = permeation coefficient of species *i*, mol/ s cm bar

Super/Subscripts

* = reference state

0 = solvent

1 = electronically conducting phase

2 = ionically conducting phase

O = oxidant

R = reductant

References

[1] N. R. C. "Committee for the National Academies Summit on America's Energy Future, *The National Academies Summit on America's Energy Future: Summary of a Meeting*(National Academies Press, Washington, DC, 2008).

[2] "Energy Storage Technology Valuation Primer: Techniques for Financial Modeling," EPRI Report 1008810, Palo Alto, California 1008810, December 2004 2004.

[3] A. Price, *Proceedings of the Institution of Civil Engineers-Civil Engineering,* **158**, 52 (2005).

[4] "Handbook of Energy Storage for Transmission or Distribution Applications," EPRI Report 1007189, Palo Alto, CA2002.

[5] C. Ponce De Leon, A. Frias-Ferrer, J. Gonzalez-Garcia, D. Szanto, and F. C. Walsh, *Journal of Power Sources,* **160**, 716 (2006).

[6] X. Li, H. Zhang, Z. Mai, and I. Vankelecom, *Energy Environ. Sci.,* (2011).

[7] M. Skyllas-Kazacos, M. H. Chakrabarti, S. A. Hajimolana, F. S. Mjalli, and M. Saleem, *Journal of the Electrochemical Society,* **158**, R55 (2011).

[8] Z. G. Yang, J. L. Zhang, M. C. W. Kintner-Meyer, X. C. Lu, D. W. Choi, J. P. Lemmon, and J. Liu, *Chemical Reviews,* **111**, 3577 (2011).

[9] P. C. Symons and P. C. Butler, "Advanced Batteries for Electric Vehicles and Emerging Applications - Introduction," in *Hnadbook of Batteries, 3rd Edition*, D. Linden and T. B. Reddy, Eds., ed New York: McGraw-Hill, 2002.

[10] J. K. Kaldellis and D. Zafirakis, *Energy,* **32**, 2295 (2007).

[11] Y. V. Makarov, C. Loutan, J. Ma, and P. De Mello, *IEEE T. Power Syst.,* **24**, 1039 (2009).

[12] Departmentofenergyofficeofelectricitydeliveryandenergyreliability. (2011, May). Available: http://www.oe.energy.gov/

[13] Departmentofenergy. (2009, May). *President Obama Announces $3.4 Billion Investment to Spur Transition to Smart Grid.* Available: http://www.energy.gov/news2009/8216.html

[14] N. Group", "Advanced Materials and Devices for Stationary Electrical Energy Storage Applications," 2010.

[15] E. A. Committee", "Bottling Electricity: Storage as a Strategic Tool for Managing Variability and Capacity Concerns in the Modern Grid," 2008.

[16] M. Skyllas-Kazacos and F. Grossmith, *Journal of the Electrochemical Society,* **134**, 2950 (1987).

[17] R. J. Remick and P. G. P. Ang, "Electrically Rechargeable Anionically Active Reduction-Oxidation Electrical Storage-Supply System," USA Patent 4,485,154, November 27, 1984, 1984.

[18] H. T. Zhou, H. M. Zhang, P. Zhao, and B. L. Yi, *Electrochim. Acta,* **51**, 6304 (2006).

[19] L. H. Thaller, *NASA TM-X-71540,* (1974).

[20] L. H. Thaller, *NASA TM-79143, DOE/NASA/1002-79/3,,* (1979).

[21] M. Bartolozzi, *J. Power Sources,* **27**, 219 (1989).

[22] F. Walsh, *Pure and applied chemistry,* **73**, 1819 (2001).
[23] A. Price, S. Bartley, S. Male, and G. Cooley, *Power Engineering Journal,* **13**, 122 (1999).
[24] P. Lessner, F. Mclarnon, J. Winnick, and E. Cairns, *Journal of Applied Electrochemistry,* **22**, 927 (1992).
[25] M. Skyllas-Kazacos, M. Rychcik, R. G. Robins, A. G. Fane, and M. A. Green, *Journal of the Electrochemical Society,* **133**, 1057 (1986).
[26] M. Skyllas Kazacos, M. Rychick, and R. G. Robins, "All-Vanadium Redox Battery," United States of America Patent, 1988.
[27] E. Sum, M. Rychcik, and M. Skyllas-Kazacos, *Journal of Power Sources,* **16**, 85 (1985).
[28] E. Sum and M. Skyllas-Kazacos, *Journal of Power Sources,* **15**, 179 (1985).
[29] M. Kazacos, M. Cheng, and M. Skyllas-Kazacos, *Journal of Applied Electrochemistry,* **20**, 463 (1990).
[30] M. Skyllas-Kazacos, D. Kasherman, D. Hong, and M. Kazacos, *Journal of Power Sources,* **35**, 399 (1991).
[31] F. Rahman and M. Skyllas-Kazacos, *Journal of Power Sources,* **72**, 105 (1998).
[32] M. Skyllas-Kazacos, C. Peng, and M. Cheng, *Electrochemical and solid-state letters,* **2**, 121 (1999).
[33] N. Kausar, R. Howe, and M. Skyllas-Kazacos, *Journal of Applied Electrochemistry,* **31**, 1327 (2001).
[34] C. M. Hagg and M. Skyllas-Kazacos, *Journal of Applied Electrochemistry,* **32**, 1063 (2002).
[35] T. Sukkar and M. Skyllas-Kazacos, *Journal of Membrane Science,* **222**, 235 (2003).
[36] T. Sukkar and M. Skyllas-Kazacos, *Journal of Applied Electrochemistry,* **34**, 137 (2004).
[37] F. Rahman and M. Skyllas-Kazacos, *Journal of Power Sources,* **189**, 1212 (2009).
[38] M. Skyllas Kazacos, G. Kazacos, G. Poon, and H. Verseema, *International Journal of Energy Research,* **34**, 182 (2010).
[39] M. Vijayakumar, S. D. Burton, C. Huang, L. Li, Z. Yang, G. L. Graff, J. Liu, J. Hu, and M. Skyllas-Kazacos, *Journal of Power Sources,* **195**, 7709 (2010).
[40] J. Chen, Q. Wang, and B. Wang, *Modern Chem. Ind.,* **null**, 26 (2006).
[41] A. Shibata and K. Sato, *Power Engineering Journal,* **13**, 130 (1999).
[42] T. K. Shigematsu, T.; Deguchi, H.; Hara, T.; , "Applications of a Vanadium Redox-Flow Battery to Maintain Power Quality," presented at the Transmission and Distribution Conference and Exhibition 2002: Asia Pacific. IEEE/PES, 2002.
[43] T. Mohammadi, S. Chieng, and M. Skyllas Kazacos, *Journal of Membrane Science,* **133**, 151 (1997).
[44] T. Mohammadi and M. S. Kazacos, *Journal of Applied Electrochemistry,* **27**, 153 (1997).
[45] S. Miyake and N. Tokuda, "Battery Diaphragm," ed: Google Patents, 2002.
[46] T. D. J. Hennessy, "Telecommunication System Incorporating a Vanadium Redox Battery Energy Storage System," ed: Google Patents, 2007.
[47] P. Zhao, H. Zhang, H. Zhou, J. Chen, S. Gao, and B. Yi, *Journal of Power Sources,* **162**, 1416 (2006).

[48] M. Skyllas-Kazacos, *Journal of Power Sources,* **124**, 299 (2003).
[49] M. Skyllas-Kazacos, C. Menictas, and M. Kazacos, *J. Electrochem. Soc.,* **143**, L86 (1996).
[50] M. Skyllas-Kazacos and Y. Limantari, *J. Appl. Electrochem.,* **34**, 681 (2004).
[51] H. Vafiadis and M. Skyllas-Kazacos, *Journal of Membrane Science,* **279**, 394 (2006).
[52] B. J. Chang, C. P. Garcia, D. W. Johnson, D. J. Bents, V. J. Scullin, and I. J. Jakupca, *Journal of Fuel Cell Science and Technology,* **4**, 497 (2007).
[53] S. A. Grigoriev, P. Millet, V. I. Porembsky, and V. N. Fateev, *International Journal of Hydrogen Energy,* **36**, 4164 (2011).
[54] X. J. Li, Y. Xiao, Z. G. Shao, and B. L. Yi, *Journal of Power Sources,* **195**, 4811 (2010).
[55] F. Mitlitsky, B. Myers, and A. H. Weisberg, *Energy & Fuels,* **12**, 56 (1998).
[56] K. C. Neyerlin, W. B. Gu, J. Jorne, and H. A. Gasteiger, *Journal of the Electrochemical Society,* **153**, A1955 (2006).
[57] J. T. Kim and J. Jorne, *Journal of the Electrochemical Society,* **124**, 1473 (1977).
[58] J. A. Kosek and A. B. Laconti, *Journal of Power Sources,* **22**, 293 (1988).
[59] V. Livshits, A. Ulus, and E. Peled, *Electrochemistry Communications,* **8**, 1358 (2006).
[60] K. J. Cathro, K. Cedzynska, and D. C. Constable, *J. Power Sources,* **19**, 337 (1987).
[61] M. J. Mader and R. White, *Journal of the Electrochemical Society,* **133**, 1297 (1986).
[62] M. Hromadova and W. Ronald Fawcett, *Journal of Physical Chemistry A,* **105**, (2001).
[63] H. S. Lim, A. M. Lackner, and R. C. Knechtli, *Journal of the Electrochemical Society,* **124**, 1154 (1977).
[64] R. Ltd., (2011).
[65] J. Jorne, J. T. Kim, and D. Kralik, *Journal of Applied Electrochemistry,* **9**, 573 (1979).
[66] D. Linden and T. B. Reddy, *Handbook of Batteries*, 2002).
[67] R. Zito, US Patent 3719526, 1973.
[68] L. W. Hruska and R. F. Savinell, *Journal of the Electrochemical Society,* **128**, 18 (1981).
[69] B. D. R.L. Clarke, S. Harrion, P.J. Millington, S. Mohanta, "Cerium Batteries," U.S. Patent, 2009.
[70] P. Ltd.". (2011, *Http://Plurionsystems.Com/Tech_Flow_Advantages.Html*. Available: http://plurionsystems.com/tech_flow_advantages.html
[71] P. Leung, C. P. De León, and F. Walsh, *Electrochemistry Communications,* (2011).
[72] T. Raju and C. A. Basha, *Industrial & Engineering Chemistry Research,* **47**, 8947 (2008).
[73] T. R. Crompton, Ed., *Elsevier Science and Technology Books, Vol. 14, 3rd Ed.* . Boston: Oxford, U.K., 2000, p.^pp. Pages.
[74] B. Fang, S. Iwasa, Y. Wei, T. Arai, and M. Kumagai, *Electrochim. Acta,* **47**, 3971 (2002).

[75] Y. Matsuda, K. Tanaka, M. Okada, Y. Takasu, M. Morita, and T. Matsumura-Inoue, *Journal of Applied Electrochemistry,* **18**, 909 (1988).
[76] M. Chakrabarti, R. Dryfe, and E. Roberts, *Electrochim. Acta,* **52**, 2189 (2007).
[77] T. Yamamura, Y. Shiokawa, H. Yamana, and H. Moriyama, *Electrochim. Acta,* **48**, 43 (2002).
[78] Q. Liu, A. E. S. Sleightholme, A. A. Shinkle, Y. Li, and L. T. Thompson, *Electrochemistry Communications,* **11**, 2312 (2009).
[79] Q. Liu, A. A. Shinkle, Y. Li, C. W. Monroe, L. T. Thompson, and A. E. S. Sleightholme, *Electrochemistry Communications,* **12**, 1634 (2010).
[80] A. E. S. Sleightholme, A. A. Shinkle, Q. Liu, Y. Li, C. W. Monroe, and L. T. Thompson, *Journal of Power Sources,* **196**, 5742 (2011).
[81] A. A. Shinkle, A. E. S. Sleightholme, L. D. Griffith, L. T. Thompson, and C. W. Monroe, *Journal of Power Sources,* in press (2011).
[82] A. Kraytsberg and Y. Ein-Eli, *Journal of Power Sources,* **196**, 886 (2011).
[83] Y. Chiang, C. Carter W, B. Ho, and M. Duduta, "High Energy Density Redox Flow Device," ed: WO Patent WO/2009/151,639, 2009.
[84] M. Duduta, Ho, B., Wood, V. C., Limthongkul, P., Brunini, V. E., Craig Carter, W. And Chiang, Y.-M. . , *Advanced Energy Materials,* **1**, (2011).
[85] K. J. Vetter, *Electrochemical Kinetics: Theoretical and Experimental Aspects*(Academic Press, New York and London, 1967).
[86] A. J. Bard and L. R. Faulkner, *Electrochemical Methods: Fundamentals and Applications*(Wiley, Hoboken, NJ, 2000).
[87] H. Gerischer, *Z Physik Chem. Neue Forschung,* **26**, (1960).
[88] M. D. Newton and J. F. Smalley, *Phys. Chem. Chem. Phys,* **9**, 325 (2007).
[89] A. J. Bard, *Journal of the American Chemical Society,* **132**, 7559 (2010).
[90] Z. Nagy, N. C. Hung, and R. M. Yonco, *Journal of the Electrochemical Society,* **138**, 2032 (1991).
[91] J. E. B. Randles and K. W. Somerton, *Transactions of the Faraday Society,* **48**, 937 (1952).
[92] M. Gattrell, J. Qian, C. Stewart, P. Graham, and B. Macdougall, *Electrochim. Acta,* **51**, 395 (2005).
[93] S. Zhong, M. Kazacos, R. Burford, and M. Skyllas-Kazacos, *Journal of Power Sources,* **36**, 29 (1991).
[94] G. Faita, G. Fiori, and T. Mussini, *Electrochim. Acta,* **13**, 1765 (1978).
[95] M. Mastragostino and C. Gramellini, *Electrochim. Acta,* **30**, 373 (1985).
[96] V. Haddadi-Asl, M. Kazacos, and M. Skyllas-Kazacos, *Journal of Applied Electrochemistry,* **25**, 29 (1995).
[97] P. Han, H. Wang, Z. Liu, X. Chen, W. Ma, J. Yao, Y. Zhu, and G. Cui, *Carbon,* **49**, 693 (2011).
[98] N. C. Hung and Z. Nagy, *Journal of the Electrochemical Society,* **134**, 2215 (1987).
[99] K. Kinoshita, *Carbon. Electrochemical and Physiochemical Properties*(John Wiley and Sons, New York, 1988).
[100] D. R. Rosseinsky, *Chemical Reviews,* **65**, 467 (1965).
[101] M. Inoue, Y. Tsuzuki, Y. Iizuka, and M. Shimada, *J. Electrochem. Soc.;(United States),* **134**, (1987).

[102] C. P. De Leon, G. W. Reade, I. Whyte, S. E. Male, and F. C. Walsh, *Electrochim. Acta,* **52**, 5815 (2007).
[103] L. H. Thaller, "Electrically Rechargable Redox Flow Cell," 3996064, 1976.
[104] "Energy Independence and Security Act of 2007," in *110-140*, ed. United States of America, 2007.
[105] Y. Y. Shao, X. Q. Wang, M. Engelhard, C. M. Wang, S. Dai, J. Liu, Z. G. Yang, and Y. H. Lin, *Journal of Power Sources,* **195**, 4375 (2010).
[106] Y. M. Chiang and R. Bazzarella, "Fuel System Using Redox Flow Battery," ed: WO Patent WO/2010/118,060, 2010.
[107] J. Van Brakel and P. M. Heertjes, *International Journal of Heat and Mass Transfer,* **17**, 1093 (1974).
[108] R. Carta, S. Palmas, A. M. Polcaro, and G. Tola, *Journal of Applied Electrochemistry,* **21**, 793 (1991).
[109] F. a. L. Dullien, *Porous Media: Fluid Transport and Pore Structure*, 2nd ed.(Academic Press, Inc., New York, 1992).
[110] J. T. Gostick, M. W. Fowler, M. D. Pritzker, M. A. Ioannidis, and L. M. Behra, *Journal of Power Sources,* **162** 228 (2006).
[111] J. Newman, *Journal of the Electrochemical Society,* **142**, 97 (1995).
[112] A. Roy, M. A. Hickner, B. R. Einsla, W. L. Harrison, and J. E. Mcgrath, *Journal of Polymer Science Part a-Polymer Chemistry,* **47**, 384 (2009).
[113] M. Sankir, Y. S. Kim, B. S. Pivovar, and J. E. Mcgrath, *Journal of Membrane Science,* **299**, 8 (2007).
[114] J. T. Gostick, M. A. Ioannidis, M. W. Fowler, and M. D. Pritzker, "Characterization of the Capillary Properties of Gas Diffusion Media," in *Modern Aspects of Electrochemistry*. vol. 49, C. Y. Wang and U. Pasaogullari, Eds., ed Berlin: Springer, 2010.
[115] J. Newman and K. E. Thomas-Alyea, *Electrochemical Systems*, 3rd ed.(John Wiley & Sons, New York, 2004).
[116] R. B. Bird, W. E. Stewart, and E. N. Lightfoot, *Transport Phenomena*, 2nd ed.(John Wiley & Sons, Inc., New York, 2002).
[117] A. Einstein, *Ann. Physik.,* **17**, 549 (1905).
[118] W. Nernst, *Zeitschrift fuer Physikalische Chemie,* **2**, 613 (1888).
[119] A. Z. Weber and J. Newman, *Chemical Reviews,* **104**, 4679 (2004).
[120] J. Bear, *Dynamics of Fluids in Porous Media*(Dover Publications, Inc., New York, 1988).
[121] Y. W. D. Chen and A. J. Bard, *Inorganic Chemistry,* **23**, 2175 (1984).
[122] B. Sun and M. Sykllaskazacos, *Electrochim. Acta,* **37**, 1253 (1992).
[123] P. Zhao, H. M. Zhang, H. T. Zhou, and B. L. Yi, *Electrochim. Acta,* **51**, 1091 (2005).
[124] B. Sun and M. Skyllaskazacos, *Electrochim. Acta,* **37**, 2459 (1992).
[125] L. Joerissen, J. Garche, C. Fabjan, and G. Tomazic, *Journal of Power Sources,* **127**, 98 (2004).
[126] M. M. E. Duarte, A. S. Pilla, J. M. Sieben, and C. E. Mayer, *Electrochemistry Communications,* **8**, 159 (2006).
[127] A. Yan, X. Xiao, I. Kulaots, B. W. Sheldon, and R. H. Hurt, *Carbon,* **44**, 3116 (2006).

[128] R. Sioda, *Electrochim. Acta,* **22**, 439 (1977).
[129] J. Cano and U. Böhm, *Chemical Engineering Science,* **32**, 213 (1977).
[130] L. Li, S. Kim, W. Wang, M. Vijayakumar, Z. Nie, B. Chen, J. Zhang, G. Xia, J. Hu, and G. Graff, *Advanced Energy Materials,* (2011).
[131] P. Ridgway, K. Cho, V. S. Battaglia, A. Z. Weber, and V. Srinivasan, "Redox Kinetics of the Bromine-Bromide Reaction for Flow Batteries " presented at the 220th Meeting of the Electrochemical Society, Boston, MA, 2011.
[132] C. Horne, K. Kinoshita, and D. B. Hickey, "Redox Flow Battery System for Distributed Energy Storage," United States Patent 12/498103, 2010.
[133] C. R. Schroll, "Manifold Dielectric Barrier for a Fuel Cell Electrical Power Generation System," United States of America Patent, 1984.
[134] M. Katz, *Journal of the Electrochemical Society,* **125**, 515 (1978).
[135] G. Zhou, L. Chen, and J. Seaba, *Proceedings of the 4th International ASME Conference on Fuel Cell Science, Engineering, and Technology, Pts A and B,* 863 (2006).
[136] presented at the Arpa-e Energy Summit, 2011.
[137] G. Codina and A. Aldaz, *Journal of Applied Electrochemistry,* **22**, 668 (1992).
[138] G. Codina, J. R. Perez, M. Lopezatalaya, J. L. Vazquez, and A. Aldaz, *Journal of Power Sources,* **48**, 293 (1994).
[139] K. Kanari, K. Nozaki, H. Kaneko, T. Hashimoto, and T. Fujii, *Denki Kagaku,* **59**, 237 (1991).
[140] K. A. Mauritz and R. B. Moore, *Chemical Reviews,* **104**, 4535 (2004).
[141] A. Z. Weber and J. Newman, *Journal of the Electrochemical Society,* **151**, A311 (2004).
[142] P. N. Pintauro and D. N. Bennion, *Industrial & Engineering Chemistry Fundamentals,* **23**, 230 (1984).
[143] A. Z. Weber and C. Delacourt, *Fuel Cells,* **8**, 459 (2008).
[144] C. Delacourt and J. Newman, *Journal of the Electrochemical Society,* **155**, B1210 (2008).
[145] J. Xi, Z. Wu, X. Qiu, and L. Chen, *Journal of Power Sources,* **166**, 531 (2007).
[146] X. Teng, Y. Zhao, J. Xi, Z. Wu, X. Qiu, and L. Chen, *Journal of Power Sources,* **189**, 1240 (2009).
[147] C. Jia, J. Liu, and C. Yan, *Journal of Power Sources,* **195**, 4380 (2010).
[148] J. Qiu, M. Zhai, J. Chen, Y. Wang, J. Peng, L. Xu, J. Li, and G. Wei, *Journal of Membrane Science,* **342**, 215 (2009).
[149] J. Qiu, L. Zhao, M. Zhai, J. Ni, H. Zhou, J. Peng, J. Li, and G. Wei, *Journal of Power Sources,* **177**, 617 (2008).
[150] D. Chen, S. Wang, M. Xiao, and Y. Meng, *Journal of Power Sources,* **195**, 2089 (2010).
[151] D. Chen, S. Wang, M. Xiao, and Y. Meng, *Energy Conversion and Management,* (2010).
[152] D. Chen, S. Wang, M. Xiao, and Y. Meng, *Energy Environ. Sci.,* **3**, 622 (2009).
[153] X. Teng, Y. Zhao, J. Xi, Z. Wu, X. Qiu, and L. Chen, *Journal of Membrane Science,* **341**, 149 (2009).
[154] S. Sang, Q. Wu, and K. Huang, *Journal of Membrane Science,* **305**, 118 (2007).

[155] Q. Luo, H. Zhang, J. Chen, P. Qian, and Y. Zhai, *Journal of Membrane Science,* **311**, 98 (2008).
[156] J. Newman and W. Tiedemann, *AIChE Journal,* **21**, 25 (1975).
[157] L. Yue, W. S. Li, F. Q. Sun, L. Z. Zhao, and L. D. Xing, *Carbon,* **48**, 3079 (2010).
[158] J. A. Trainham and J. Newman, *Journal of the Electrochemical Society,* **124**, 1528 (1977).
[159] J. A. Trainham and J. Newman, *Journal of Applied Electrochemistry,* **7**, 287 (1977).
[160] J. A. Trainham and J. Newman, *Journal of the Electrochemical Society,* **125**, 58 (1978).
[161] P. S. Fedkiw and R. W. Watts, *Journal of the Electrochemical Society,* **131**, 701 (1984).
[162] M. Lopez-Atalaya, G. Codina, J. Perez, J. Vazquez, and A. Aldaz, *Journal of Power Sources,* **39**, 147 (1992).
[163] H. Al-Fetlawi, A. A. Shah, and F. C. Walsh, *Electrochim. Acta,* **55**, 78 (2009).
[164] H. Al-Fetlawi, A. A. Shah, and F. C. Walsh, *Electrochim. Acta,* **55**, 3192 (2010).
[165] K. Knehr and E. Kumbur, *Electrochemistry Communications,* (2011).
[166] A. Shah, H. Al-Fetlawi, and F. Walsh, *Electrochim. Acta,* **55**, 1125 (2010).
[167] A. Shah, R. Tangirala, R. Singh, R. G. A. Wills, and F. C. Walsh, *Journal of the Electrochemical Society,* **158**, A671 (2011).
[168] M. Vynnycky, *Energy,* **36**, 2242 (2011).
[169] D. You, H. Zhang, and J. Chen, *Electrochim. Acta,* **54**, 6827 (2009).
[170] A. Shah, M. Watt-Smith, and F. Walsh, *Electrochim. Acta,* **53**, 8087 (2008).
[171] H. Al-Fetlawi, A. Shah, and F. Walsh, *Electrochim. Acta,* **55**, 3192 (2010).
[172] M. Li and T. Hikihara, *Ieice Transactions on Fundamentals of Electronics Communications and Computer Sciences,* **E91A**, 1741 (2008).
[173] D. P. Scamman, G. W. Reade, and E. P. L. Roberts, *Journal of Power Sources,* **189**, 1220 (2009).
[174] D. P. Scamman, G. W. Reade, and E. P. L. Roberts, *Journal of Power Sources,* **189**, 1231 (2009).
[175] T. I. Evans and R. E. White, *Journal of the Electrochemical Society,* **134**, 2725 (1987).
[176] R. Putt, "Assessment of Technical and Economic Feasibility of Zinc/Bromine Batteries for Utility Load-Levelling, Epri Report Em-1059, Project 635-1, Palo Alto, Ca, Appendix M," 1979.
[177] J. Lee and J. Selman, *Journal of the Electrochemical Society,* **129**, 1670 (1982).
[178] J. Jorne, *Journal of the Electrochemical Society,* **129**, 2251 (1982).
[179] E. Roayaie and J. Jorne, *Journal of the Electrochemical Society,* **132**, 1273 (1985).
[180] P. Trinidad, C. P. De Leon, and F. Walsh, *Journal of environmental management,* **88**, 1417 (2008).